Energy & Environmental Science

RSC Publishing

REVIEW

View Article Online
View Journal | View Issue

Cite this: *Energy Environ. Sci.*, 2013, **6**, 1388

Graphene-based electrodes for electrochemical energy storage

Chaohe Xu,†[b] Binghui Xu,†[a] Yi Gu,†[a] Zhigang Xiong,[a] Jing Sun[b] and X. S. Zhao*[ac]

Received 23rd October 2012
Accepted 11th March 2013

DOI: 10.1039/c3ee23870a

www.rsc.org/ees

The ever-increasing demands for energy and environmental concerns due to burning fossil fuels are the key drivers of today's R&D of innovative energy storage systems. This paper provides an overview of recent research progress in graphene-based materials as electrodes for electrochemical energy storage. Beginning with a brief description of the important properties of single-layer graphene, methods for the preparation of graphene and its derivatives (graphene oxide and reduced graphene oxide) are summarized. Then, graphene-based electrode materials for electrochemical capacitors and lithium-ion batteries are reviewed. The use of graphene for improving the performance of lithium–sulfur and lithium–oxygen batteries is also presented. Future research trend in the development of high-power-density and high-energy-density electrochemical energy storage devices is analysed.

Broader context

The ever-increasing demands for energy and environmental issues due to consumption of fossil fuels are the key drivers of today's R&D of innovative energy storage systems. The development of high-performance energy storage systems that can deliver energy with a high power rate is critical for future success in global efforts on sustainable and renewable energy. Over the past ten years or so, graphene-based electrode materials have been extensively studied for these devices. This review presents a comprehensive summary of the fundamental properties of graphene, general methods for preparing graphene and its derivatives, and applications as electrode materials for electrochemical energy storage devices, including supercapacitors (SCs), lithium-ion batteries (LIBs), lithium–sulfur (Li–S) batteries, and lithium–oxygen (Li–O_2) batteries.

1 Introduction

Graphene is a single layer of sp^2 carbon atoms arranged hexagonally. Graphene has a high intrinsic carrier mobility (200 000 $cm^2\ V^{-1}\ s^{-1}$),[1] excellent thermal conductivity (~5000 $W\ m^{-1}\ K^{-1}$),[2–4] high optical transmittance (~97.7%),[5] high theoretical specific surface area (2630 $m^2\ g^{-1}$),[6] and superior mechanical strength.[1] Thus, graphene is envisioned to find a wide spectrum of applications.[7–16] As graphite consists of single graphene layers connected *via* van der Waals forces, it is not unexpected that graphene can be produced by exfoliation of graphite physically[17] or chemically.[18,19] The chemical exfoliation approach, however, generally yields a chemically modified graphene, which has a significantly lower electric conductivity than pristine graphene.[20] In the chemical exfoliation method, highly oxidative chemicals are used to loosen the van der Waals forces between graphene layers in graphite, leading to the formation of graphite oxide, which contains a substantial amount of oxygen-containing groups. Exfoliation of the graphite oxide using mechanical means (*e.g.*, ultrasonication) yields graphene oxide (GO). Reduction of GO chemically or thermally produces reduced graphene oxide (RGO), which, however, still contains oxygen species, especially at the edges of the RGO sheets.[21] Because it is easy and inexpensive, the chemical exfoliation method has been widely used in research labs worldwide to make graphene samples. Strictly speaking, the chemical exfoliation approach does not yield graphene, but graphene derivatives (*e.g.*, GO and RGO). Nevertheless, graphene and RGO are used interchangeably in many cases, as in this review.

With the ever-aggravating environmental impacts of consuming fossil fuels, sustainable energy production, storage, management, and consumption are gaining more and more attention.[22,23] The development includes not only technologies for harvesting and converting sustainable energy sources, but also effective methods for storing and delivering the energy efficiently upon demand for applications, such as electric vehicles and smart grids.[24] Lithium-ion batteries (LIBs) and supercapacitors (SCs) are electrochemical energy storage devices that could meet such demands. Unfortunately, neither LIBs nor SCs that are currently available in the market can fulfil the demand due to their poor performance (*e.g.*, low energy

[a]*School of Chemical Engineering, The University of Queensland, St Lucia, Brisbane, QLD 4072, Australia. E-mail: george.zhao@uq.edu.au*

[b]*The State Key Lab of High Performance Ceramics and Superfine Microstructure, Shanghai Institute of Ceramics, Chinese Academy of Sciences, 1295 Dingxi Road, Shanghai 200050, China*

[c]*Institute of Multifunctional Materials, Qingdao University, 38 Ningxia Road, Qingdao, China*

† C. Xu, B. Xu and Y. Gu contributed equally.

density for SCs, low power rate and short lifetime for LIBs). As a result, the past few years have seen a great deal of research effort in improving the performance of these energy storage devices.

In comparison with SCs, LIBs possess a higher energy density (120–200 W h kg^{-1}), but a lower power density (lower than 500 W kg^{-1}) and shorter cycle life (less than 500 cycles).[25] While the energy density of SCs is higher than that of dielectric capacitors, it is still much lower than that of batteries and fuel cells.[26] Most of the commercially available SCs have a specific energy density of less than 10 W h kg^{-1}, about one tenth of that of LIBs. The most striking features of SCs are their high power density (1000–5000 W kg^{-1}) and long cycle life (>10^5).[27]

Rechargeable Li–oxygen (Li–O_2) and Li–sulphur (Li–S) batteries with respective theoretical specific energy densities of about 2567 and 3500 W h kg^{-1} based on the mass of Li and discharge product (Li_2O_2 or LiO_2) are gaining more and more recent research interests.[28] While Li–O_2 and Li–S batteries share the same anode, they work differently in terms of the redox chemistry of O and S.

LIBs and SCs have found applications in niche areas due to their drawbacks. For applications such as electric vehicles and smart grids, high-performance energy storage devices must be developed. Recent research advancements in the development of new-generation electrochemical energy storage devices have been largely associated with the design and availability of innovative electrode materials.[28] This review summarizes recent research progress in graphene-based electrode materials for high-performance electrochemical energy storage devices.

2 Properties of graphene

Graphene is a single layer carbon nanosheet consisting of two equivalent sub-lattices of sp^2 carbon atoms connected by σ bonds.[30] Each carbon atom in the lattice has a π orbital that contributes to a delocalized network of electrons.[31] This extraordinary chemical structure (known as the Dirac fermion system) leads graphene to display unique physical and chemical properties because of its linear energy dispersion, high electron–hole symmetry and internal degree of freedom.[32]

2.1 Physical properties

As a consequence of the graphene structure, the first Brillouin zone has two inequivalent points (Dirac points), where a band

Chaohe Xu received his PhD in Materials Physics and Chemistry from Shanghai Institute of Ceramics, Chinese Academy of Sciences (2012), and Bachelors degree in Materials Science and Engineering from Tianjin University (2007). His PhD research project focused on the design, synthesis and characterization of nanocarbon materials for Li-ion batteries and supercapacitors. His current research interests include flexible electrodes for energy storage, Li–S and Li–O_2 batteries.

Yi Gu received her BS in Chemistry from Fudan University (China) in 2007, where she proceeded with obtaining her MS in Physical Chemistry in 2010. In 2012 she received another MS in Chemical Engineering from Tufts University (USA). She is now pursuing her PhD under the supervision of Prof. X.S. Zhao at the School of Chemical Engineering, the University of Queensland (Australia). Her research project deals with designing novel carbon-based materials for electrochemical capacitors.

Binghui Xu received his B.E. from the School of Chemistry and Chemical Engineering at the Central South University in 2011. He is now a PhD candidate in the School of Chemical Engineering at the University of Queensland under the supervision of Prof. X.S. Zhao. His research interest is anode materials for lithium ion batteries.

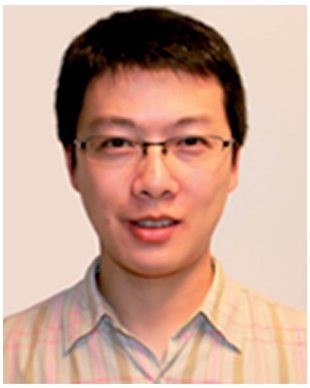

Zhigang Xiong received his PhD in chemistry from Zhejiang University (China) in 2008 under the supervision of Prof. Yiming Xu. After two and half years of postdoctoral research training in Prof. X.S. Zhao's group at the Department of Chemical and Biomolecular Engineering, National University of Singapore, he moved to Australia with Prof. Zhao in 2011 to take the same position at the School of Chemical Engineering, the University of Queensland. His current research interests are mainly focused on synthesizing semiconductor-/graphene-based composite materials and their applications in heterogeneous photocatalysis.

crossing occurs. Intrinsic single-layer graphene is a zero-gap semiconductor (Fig. 1a).[29] The electronic-band structure of graphene leads to semiconducting and metallic characteristics, thus being considered as both a metal with a vanishing Fermi surface and a semiconductor with a vanishing band gap. The room-temperature carrier mobility of graphene is as high as 15 000 $cm^2\ V^{-1}\ s^{-1}$, and the charge carriers can be tuned continuously between electrons and holes with concentrations as high as $10^{13}\ cm^{-2}$.[33,34] In addition, by minimizing impurity scattering, mobilities in excess of 200 000 $cm^2\ V^{-1}\ s^{-1}$ can be achieved in suspended graphene.[6] The electronic properties of graphene change with the number of layers and relative position of atoms in adjacent layers determined by the stacking order.[35] Bilayer graphene shows parabolic bands (no Dirac electrons), which touch the Fermi level (Fig. 1b).[29] However, under the presence of an electric field, the gap of the bilayer graphene can be opened.[17,36] Trilayer graphene shows an interesting band structure, which looks like a combination of a monolayer and a bilayer (Fig. 1c).[29,37] In general, for few-layer graphene with AB stacking, there will be a linear band if the number of layers is odd.[38–40] As the number of layers increases, the band structure becomes more complicated, leading to the appearance of several charge carriers and the overlapping of the conduction and valence bands.

The opacity of graphene is about 2.3% that is determined by its structure and electronic properties.[41] The constant transparency (of about 97%) has been experimentally observed in the visible range.[42] It has also been observed that the transmittance decreases linearly with the number of layers of graphene. Because of the superior electrical and optical properties, graphene may be a potential substitute for commercial transparent electrodes such as indium tin oxides.

The thermal conductivity of suspended graphene is extremely high, ranging from 4840 to 5300 $W\ m^{-1}\ K^{-1}$, higher than the experimentally measured values of carbon nanotubes and diamond.[2] The outstanding thermal conductivity of graphene makes it a good material for improving the thermal conductivity of polymers and ceramics. Balandin and coworkers[43,44] demonstrated that with 5 and 10 vol% doping of graphene, the thermal conductivity of graphene–metal and graphene–polymer composites was increased by about 500% and 2300%, respectively. This is attributed to the high intrinsic thermal conductivity of graphene, together with its strong coupling with the metal and polymer.[43]

Owing to the strong σ bonds (C–C bonds), monolayer graphene has superior mechanical properties, such as high Young's modulus and strong fracture strength.[31] The elastic modulus of graphene sheets prepared using the chemical exfoliation method was determined to be about 0.25 TPa.[45] The elastic modulus and intrinsic strength of a defect-free monolayer graphene were measured to be 1.0 TPa and 130 GPa,[46] respectively. Paper-like graphene films showed very high

Prof. Jing Sun received her PhD in 1997 from the Shanghai Institute of Ceramics, Chinese Academy of Sciences (SICCAS) and joined the State key Lab of High Performance Ceramics and Superfine Microstructure in the same year. Afterwards, she spent one year as a visiting scientist in the Institute for Surface Chemistry in Stockholm (YKI) between 1999 and 2000 and worked as a JSPS fellow in the National Institute of Advanced Science and Technology (AIST) in Japan during 2002–2004. In 2005, she got the support from "the Hundred Talents Program of CAS" and has been working as a full Professor in SICCAS since then. Prof. Jing Sun is heading a research group of 20 graduate students and scientists and her current research interests include: low dimensional carbon materials (including carbon nanotubes and graphene) and their composites, novel photovoltaic devices based on inorganic and organic materials, nanotubes, nanowires, and lithium ion battery materials. She has published over 130 peer-reviewed journal articles in Adv. Mater., ACS Nano, Carbon and so on. She is a co-author of the book titled "Dispersion and Characterization of Nano Powder", and organized three international conferences on materials science and technology. She has won the First Prize of Shanghai Science and Technology two times.

X.S. Zhao received his PhD in Chemical Engineering from The University of Queensland (UQ) in 1999. He then worked as a UQ Postdoctoral Research Fellow at the same university. He joined the Department of Chemical and Biomolecular Engineering, National University of Singapore, as an Assistant Professor in 2001, and then was promoted to Associate Professor in 2006. In 2010, he was awarded an Australian Research Council (ARC) Future Fellow, and appointed as a full professor by UQ. He took up the appointment and joined the School of Chemical Engineering of UQ to lead a research program of Clean Energy and Water Research. Professor Zhao's research focuses on porous materials for emerging applications. His current research projects include porous carbon and graphene electrodes for supercapacitors and lithium-ion batteries, charge storage mechanism and transport behavior in nanoporous carbon electrodes (both experimentally and computationally), novel photocatalysts for detoxification and disinfection, colloidal photonic crystals and macroporous materials, mesoporous materials for C1 utilization (methane reforming with CO_2, methanol to olefins, and CO_2 storage), and membrane separation of bio-oils.

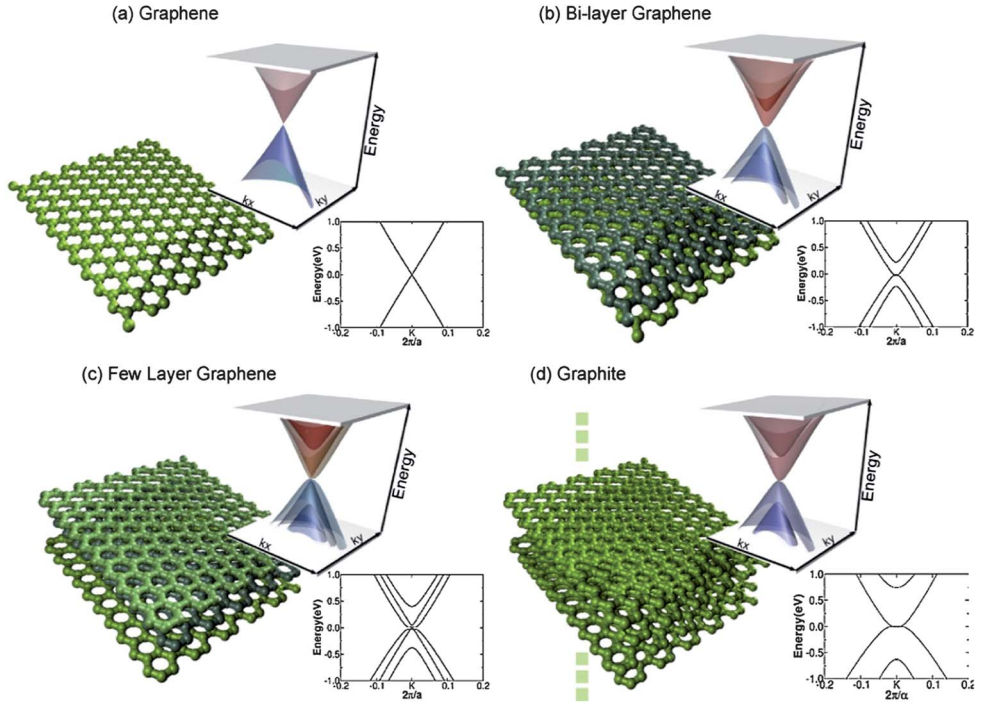

Fig. 1 Low energy DFT 3D band structure and its projection on k_x close to the k point for (a) graphene, (b) bilayer graphene, (c) trilayer graphene and (d) graphite. Monolayer graphene shows the Dirac point of graphene (a). The Dirac point is lost in bilayer graphene (b), but appears again in trilayer graphene (c); (d) shows the graphite structure which displays a semimetallic band structure with parabolic-like bands. The Fermi level has been set at zero in all cases. Reproduced with permission.[29]

hardness, about 217 kgf mm^{-2},[47] almost two times harder than that of carbon steel. Moreover, the yielding strength of graphene (about 6.4 TPa) is several times higher than that of carbon steel.[47] Kim and co-workers[48] recently studied the interplay of mechanical and electronic properties of graphene. The resistance in the bent direction increased almost one order of magnitude. The resistance change due to stretching was about one order of magnitude difference along the directions parallel and perpendicular to the stretching direction.

2.2 Chemical properties

The surface of defect-free or highly crystalline graphene appears to be chemically inert. The surface of pure graphene usually interacts with other molecules *via* physical adsorption (π–π interactions). To enable the graphene surface to be more reactive, surface defects or surface functional groups are usually introduced.[29] For example, chemical doping with atoms such as B and N and introducing functional groups such as carboxyl, carbonyl, and amine groups can tune the surface properties and the electronic properties of graphene.[49–52] GO is hydrophilic in nature,[10,36,53] thus it can be easily further processed in an aqueous system for applications, such as heterogeneous catalysis, sensor technology, and energy storage.[35,54]

3 Preparation of graphene

Large-scale preparation of graphene with controllable size still represents a key challenge in the development of graphene technology. The first successful preparation of graphene was by using the scotch-tape method to peel off graphene *via* a layer by layer technique from a highly oriented pyrolitic graphite (HOPG), followed by depositing on a silicon substrate assisted by an organic solvent.[17] This method allows one to obtain high-quality graphene with sizes of about 10 μm. However, the yield and efficiency of the scotch-type method are low.

3.1 Chemical reduction of GO

A prerequisite for exploiting most proposed applications for graphene is the availability of processable graphene in large quantities.[20] Oxidative exfoliation of natural graphite by a thermal or oxidation technique followed by chemical reduction has been considered one of the most efficient methods for low-cost and large-scale production of graphene.[55] Ruoff and Park[19] demonstrated a solution-based route involving chemical oxidation of graphite to GO, which can be readily exfoliated as individual GO sheets. The GO can be converted to RGO by chemical reduction using, for instance, hydrazine or $NaBH_4$. However, the product thus obtained often suffers from poor dispersion or irreversible agglomeration in water. In addition, the reducing agents are toxic and unstable, making the processing difficult.

Li *et al.*[20] demonstrated that RGO colloids can be prepared through electrostatic stabilization without polymeric or surfactant stabilizers. This is mainly due to the Coulomb repulsion of the negative charges which can be adjusted by pH values. Amphiphilic molecules that have been used to improve

the solubility of carbon nanotubes[56–61] have been shown to work well for enhancing the solubility of RGO sheets.[62–71] This is mainly because the hydrophobic part forms strong π–π interaction with graphene while the hydrophilic part generates electrostatic repulsions. Zhang and co-workers[72] reported a quick deoxygenation method in strong alkali solution at moderate temperatures. This acid neutralization reaction offers an exciting opportunity for large-scale production of graphene. Other reducing agents, such as L-ascorbic acid,[73] vitamin C[73,74] and sugars (glucose, sucrose, fructose, *etc.*),[75] have also been reported.

Recently, Loh *et al.*[76] described a hydrothermal dehydration method for reducing GO to stable RGO (see Fig. 2). The reduction process was believed to be analogous to the H^+ catalyzed dehydration of alcohols, where water acts as the source of H^+ for the protonation of –OH. As shown in Fig. 2, both intramolecular (a) and intermolecular (b) dehydration can occur on the edges or basal planes of GO, which are terminated by hydrogen, hydroxyl, ether, and carboxylic groups. In the case of mechanism (a), the elimination of –OH and –H can occur on the edge sites of GO, followed by the recovery of π-bonding. Compared to the reduction method using hydrazine, this hydrothermal treatment route has a number of advantages. Based on this method, a number of solvothermal methods have been developed to prepare high-quality and high-concentration RGO colloids.[77–82] Gilje *et al.*[77] reported that *N*-methyl pyrrolidone (NMP) with a high boiling point in combination with its oxygen-scavenging properties at high temperatures is a good reagent to deoxygenate GO. The RGO obtained from this method displayed an electric conductivity of 374 S m^{-1} and a C/O ratio of 5.15.

Metals such as Fe and Zn powders have also been used to reduce GO with a high efficiency.[83,84] However, a strong acid is needed to remove the excess of metals after reduction. The RGO product obtained with Fe as the reducing agent showed a C/O ratio of 7.90 and electric conductivity of 2300 S m^{-1}.[83] Ouyang and Mei[84] reported that Zn powder is a good reductant for reducing GO. The C/O atomic ratio and electric conductivity of a RGO product obtained with Zn as the reducing agent were 33.5 and 15 000 S m^{-1}, respectively.

Apart from using the elaborate reducing agents discussed above, Williams *et al.*[85] first introduced the use of semiconductor photocatalysis to reduce GO. TiO_2 is a relatively mild reductant with the conduction band around −0.5 V *versus* normal hydrogen electrode (NHE) at neutral pH.[85,86] TiO_2 is excited to generate electron–hole pairs upon ultraviolet (UV) irradiation.[87–90] The holes are scavenged by ethanol, leaving the electrons accumulated on the TiO_2 surface (reaction (1)). The accumulated photoelectron in the conduction band of TiO_2 is then trapped by GO to reduce oxygen-containing groups to form RGO (reaction (2)).

$$TiO_2 + h\nu \rightarrow TiO_2(e + hole) \xrightarrow{C_2H_5OH} TiO_2(e) + C_2H_4OH + H^+ \quad (1)$$

$$TiO_2\ (e) + GO \rightarrow TiO_2 + RGO \quad (2)$$

The photocatalytic reduction can be conducted by UV irradiation of a TiO_2 suspension first, followed by incremental addition of GO suspension,[86] or direct UV irradiation of a TiO_2 and GO mixture.[91] The reduction of GO has also been demonstrated by using other photocatalyst systems, including ZnO,[92] $H_3PW_{12}O_{40}$,[93,94] WO_3,[95] CdS,[96] $BiVO_4$ (ref. 97) and nitrogen-doped $Sr_2Ta_2O_7$ (ref. 98) under UV or visible light irradiation. Although the photocatalysis-assisted reduction method does not involve elevated temperature or toxic reducing agents, it always produces a composite solid (RGO with the photocatalyst) rather than pure RGO.

Recently, Jang *et al.*[99] reported a method which allows one to obtain a RGO suspension. As illustrated in Fig. 3, the method is based on the strong electrostatic repulsion between negatively charged RGO sheets and TiO_2 particles under appropriate pH conditions. Thus, under basic conditions, negatively charged TiO_2 and RGO sheets are stabilized in water and repel each other. Thus prepared RGO showed an electric conductivity, which is comparable to that of RGO reduced by hydrazine. The recovered TiO_2 can be reused, enabling a cost-effective, environmentally friendly approach to large-scale production of pure RGO suspensions.

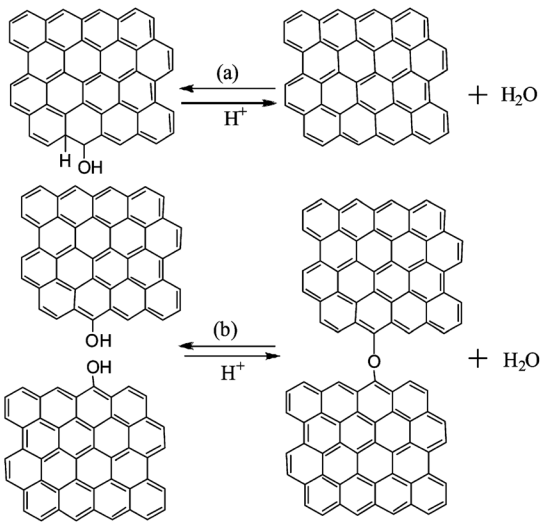

Fig. 2 (a) Intramolecular dehydration of GO under hydrothermal conditions. (b) Intermolecular dehydration of GO occurring at high pH, giving rise to aggregated products. Reproduced with permission.[76]

3.2 Chemical vapour deposition

Another approach to the preparation of graphene is *via* chemical vapour deposition (CVD), which makes use of the pyrolysis of hydrocarbon compounds on the surface of a metal catalyst at high temperatures.[100] There are two types of growth mechanisms depending on the solubility of carbon in the metal.[101] One is the carbon segregation and/or precipitation mechanism as schematically illustrated in Fig. 4a. For those catalysts with a high solubility of carbon such as Ni, the hydrocarbon compound cracks at high temperatures to form carbon species, which dissolve in the metal. Upon cooling, the carbon species precipitate out from the surface of the metal followed by

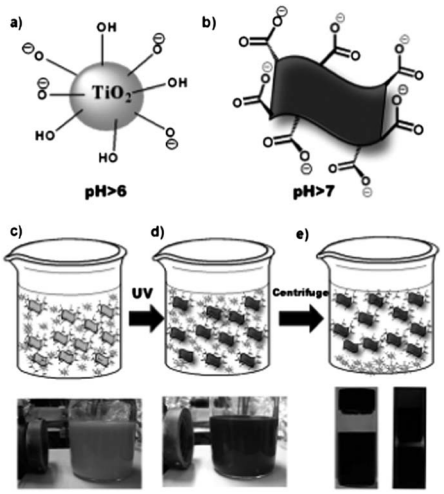

Fig. 3 Schematic illustrations of (a) a TiO_2 particle carrying negative charge above pH 6, (b) a RGO sheet carrying negative charge above pH 7, a mixture of GO and TiO_2 under basic conditions before (c) and after (d) UV irradiation for 5 h, RGO prepcipitate and TiO_2 particles in the liquid phase after ultracentrifugation (e). Reproduced with permission.[99]

nucleation and growth to form graphene. The number of graphene layers is strongly dependent on the cooling rate. Kong *et al.*[102] and Hong *et al.*[103] employed polycrystalline Ni as a catalyst to prepare graphene using the CVD method. However, it was difficult to prepare graphene with a large size and controllable morphology. The number of layers was unevenly distributed. In order to solve this problem, Cheng *et al.*[104] adopted nickel foam as the catalyst for graphene growth and successfully synthesized graphene foams with potential applications as chemical sensors and energy storage devices.[105–108] The other one is the surface growth mechanism as shown in Fig. 4b. Instead of diffusing into the matrix of metal catalysts such as Cu,[101] a carbon precursor firstly adsorbs on the surface of the catalyst, and then nucleates and grows to form a graphene island, and finally graphene by continuous growth. Ruoff *et al.*[100] used a Cu foil to grow graphene of a large domain. Ahn

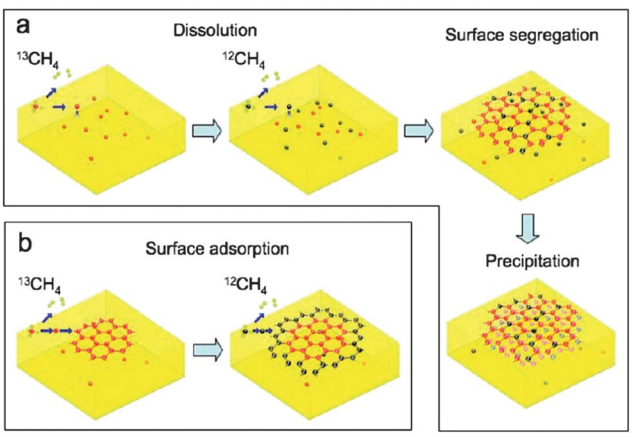

Fig. 4 Schematic illustration of the possible growth mechanisms of graphene in a CVD process: (a) the carbon segregation/precipitation mechanism and (b) the surface growth mechanism. Reproduced with permission.[101]

et al.[42] described a roll-to-roll production process and wet-chemical doping of predominantly monolayer 30-inch graphene films grown by CVD onto flexible Cu substrates. The films displayed a sheet resistance as low as ~125 Ω per square with 97.4% optical transmittance. Cheng *et al.*[109] and Kong *et al.*[110] have developed an ambient-pressure CVD route for efficient growth of graphene. The quality of graphene can be adjusted by the composition of carrier gas. In addition, both solid and liquid carbon sources have also been used to produce graphene.[111–115] Tour *et al.*[113,114] developed a one-step method for the controllable growth of pure graphene and doped graphene using solid carbon sources, such as polymethylmethacrylate (PMMA), cookies, chocolate, grass, and even wastes.

While large-domain graphene can be prepared by using the CVD method, it remains a great challenge to transfer the graphene from the catalyst substrate to another substrate. The currently used most common method for transferring graphene is etching away the metal substrate using a suitable etchant,[103,116] which inevitably leads to a number of problems, such as damage to graphene, high cost, and generation of wastes. Recently, Wang *et al.*[117] demonstrated an electrochemical delamination method to repeatedly transfer graphene from a Cu substrate to another substrate. The growth and transfer processes on the Cu substrate were repeated hundreds of times. However, the substrate was partially etched during each transfer. Very recently, Cheng *et al.*[118] reported a bubbling method to transfer graphene grains and films to an arbitrary substrate as illustrated in Fig. 5. The method is neither destructive to graphene nor to the Pt substrate. The Pt substrate can be repeatedly used and the quality of graphene grown on the recycled Pt substrate was almost identical to that grown on the initial Pt substrate.

3.3 The arc discharge method

The arc discharge method has been used for the production of fullerenes, single- and multi-walled carbon nanotubes.[119] The temperature can be instantaneously increased to over 2000 °C during the arc discharge process.[120] Therefore, it is naturally expected that arc discharge can be used for efficient exfoliation and deoxygenation of GO and healing of the resultant exfoliated graphite. Rao *et al.*[121] reported that the graphene prepared using the arc discharge method generally contained 2–4 layers in the inner wall of the arc chamber. Shi *et al.*[122] succeeded in large-scale production of graphene by using the arc discharge method in an air atmosphere instead of mixed H_2 and He. They found that the yield of graphene is greatly dependent on the pressure of the atmosphere, *i.e.*, high pressure promoted the formation of graphene, while low pressure favoured the growth of carbon nanohorns and nanospheres. The authors also found that nitrogen-doped graphene can be produced in large scale by the direct current arc discharge between pure graphite rods using NH_3 as one of the buffer gases.[123] In addition, hydrogen arc discharge as a rapid heating method has also been demonstrated for producing graphene from a GO dispersion.[120,124] The obtained graphene exhibited a high electrical conductivity and high thermal stability compared with the conventional thermal exfoliation method. These demonstrate that the arc discharge

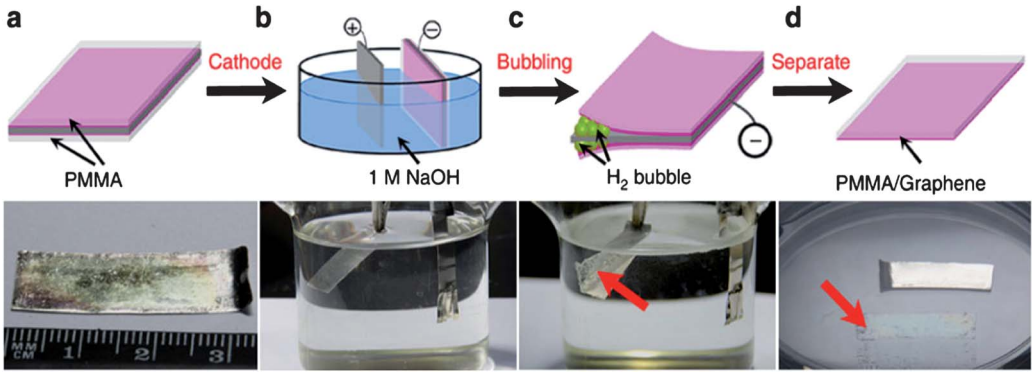

Fig. 5 Illustration of the bubbling transfer process of graphene from a Pt substrate. Reproduced with permission.[118]

exfoliation method is a good approach to the preparation of graphene with a high quality.

3.4 The ball milling approach

High-energy ball milling is an effective method to prepare few-layer graphene and its composites.[125–128] Fan *et al.*[126] developed a ball milling route to prepare graphene–Al_2O_3 composites from expanded graphite with a thickness of 2.5–20 nm. Very recently, Dai and co-workers[129] achieved a high yield of edge-selectively carboxylated graphite (ECG) by using ball-milling of graphite in the presence of dry ice (Fig. 6). The ECG is highly dispersible in various solvents to self-exfoliate into single- and few-layer (≤5 layers) graphene. This progress provides a simple, efficient, versatile, and eco-friendly approach to low-cost mass production of high-quality graphene.

3.5 Solvent-assisted exfoliation

Solvent-assisted exfoliation is an effective method to prepare two-dimensional materials.[130–133] Coleman *et al.*[130,132–134] demonstrated that when graphite powder was exposed to ultrasonication in the presence of a suitable solvent, the powder fragmented into nanosheets, which were stabilized against aggregation by the solvent. The mixing enthalpy is minimized for solvents with surface energies close to that of graphene (~68 mJ m^{-2}). The exfoliated nanosheets are free of defects and oxygen-containing groups. However, the solvent-assisted exfoliation method has some critical issues, such as low concentration of suspension, difficulty in obtaining single-layer graphene with a high yield, and high cost of some solvents.

The electrochemical exfoliation method has also been demonstrated to be an effective approach to producing high-quality graphene.[135–137] However, it is difficult to implement large-scale production of graphene by using this method because of the limited volume of electrochemical chambers or devices.

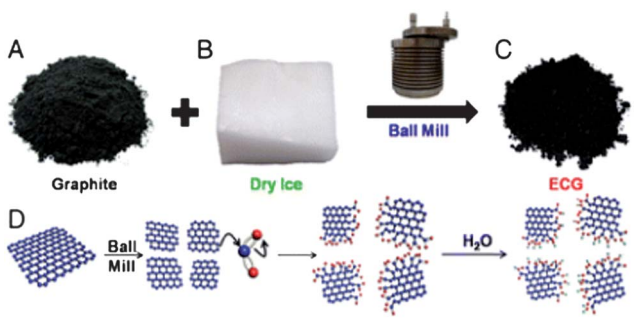

Fig. 6 Illustration of edge-carboxylation of graphite for graphene in the presence of dry ice. (A) Pristine graphite; (B) dry ice (solid phase CO_2); (C) ECG prepared by ball milling; (D) schematic representation of physical cracking and edge-carboxylation of graphite by ball milling in the presence of dry ice. Reproduced with permission.[129]

3.6 The chemical synthesis approach

As graphene is composed of polycyclic hydrocarbon rings, chemical synthesis from aromatic compounds may provide an effective route for controllable synthesis of graphene.[138–140] Indeed, Cai *et al.*[140] succeeded in synthesizing atomically precise graphene nanoribbons with different topologies and widths. The formation mechanism is illustrated in Fig. 7. Surface-assisted coupling of the molecular precursor resulted in formation of linear polyphenylenes followed by subsequent cyclodehydrogenation to form graphene nanoribbons. The authors also found that the topology, width and edge periphery of the graphene products were determined by the structure of the monomer. Interestingly, this method has been used to fabricate graphene-based devices directly, such as photovoltaics and magnetic devices.[141–143]

Stride *et al.*[144] demonstrated that single-layer graphene can be synthesized by flash pyrolysis of a solvothermal product of sodium and ethanol, followed by gentle sonication of the nanoporous carbon products. This process mainly uses the high reductive ability and chemical activity of alkali metals (*e.g.*, sodium and potassium) to produce carbon radicals, which then couple with each other to form graphene. The ability to produce bulk graphene from non-graphitic precursors with scalability and low-cost is a step closer to real applications of graphene.

4 Graphene-based electrodes for electrochemical capacitors

Tremendous efforts in SC research have been made at finding innovative electrode materials for increasing the energy density

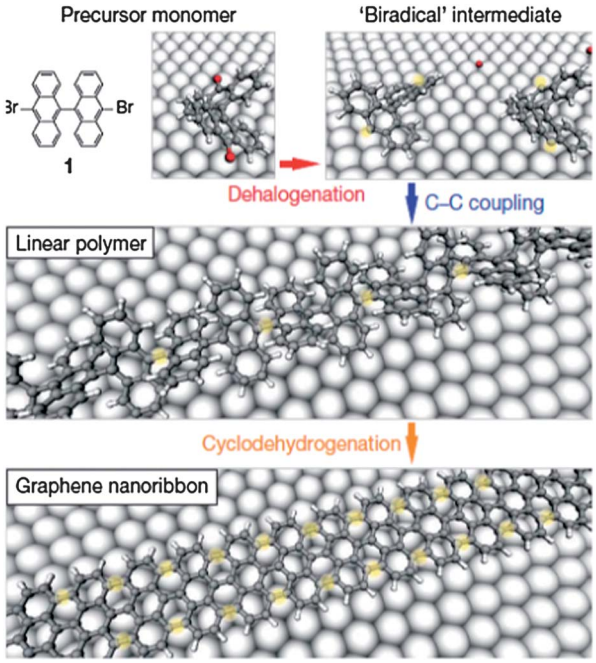

Fig. 7 A scheme showing the formation of atomically precise graphene nanoribbons from an aromatic compound. Reproduced with permission.[140]

and lowering the cost.[22–24,26] Porous carbon materials are often the choice of the electrode because of their good electrical conductivity coupled with a large interface area. Graphene has a theoretically high surface area, very high intrinsic electrical conductivity in plane, good chemical stability as well as high mechanical strength, thus it is an excellent candidate for advanced electrode materials for SCs. It is thus not unexpected that graphene and its composites have become the most studied electrode materials in recent years.

4.1 The working principle of SCs

The most striking features of SCs include high power density and long cycle life. The main weakness of SCs is their poor energy density. There are two types of capacitance – one is the electrical double layer (EDL) capacitance and the other is the pseudocapacitance. The EDL capacitance arises from the charge separation at the electrolyte/electrode interface, whereas the pseudocapacitance is caused by Faradaic reactions occurring at the interface of the electrolyte/electrode or near the surface of the electrode material. Because of these two different energy storage mechanisms, there are two types of electrochemical capacitors, namely EDL capacitors (EDLCs) and pseudocapacitors.

The EDL capacitance can be calculated using eqn (3):[27]

$$C = \frac{\varepsilon_r \varepsilon_0}{d} A \tag{3}$$

where ε_r is the relative dielectric constant, ε_0 (in F m^{-1}) is the dielectric constant of vacuum, A (in m^2 g^{-1}) is the specific surface area of the electrode accessible to the electrolyte ions, and d (in m) is the effective thickness of the electrical double layer.

For pseudocapacitive materials, the energy storage is based on the fast and reversible redox reactions between the electrolyte and the active electrode. The electrochemical reactions occur at the interface or near the interface of electrode materials. The distance of ion transportation is very short. The voltage of capacitors changed with charge in a linear way. Therefore, the capacitance of the electrode material can be expressed by:[145]

$$C = \mathrm{d}Q/\mathrm{d}V \tag{4}$$

There are three most commonly used techniques to evaluate the electrochemical performance of SCs, *i.e.* cyclic voltammetry (CV), galvanostatic charge/discharge (GCD) and electrochemical impedance spectroscopy (EIS).

4.1.1 The CV method. The overall capacitance (C in F) from the CV method is:

$$C = \frac{\mathrm{d}Q}{\mathrm{d}V} = \frac{\mathrm{d}Q}{\mathrm{d}t}\frac{\mathrm{d}t}{\mathrm{d}V} = \frac{i}{\mathrm{d}V/\mathrm{d}t} = i/v \tag{5}$$

where i (in A) is the instantaneous current in CV, dV/dt or v (in V s^{-1}) is the scanning rate of voltage. An average C can be given by the average current (i) divided by the scanning rate as:[145,146]

$$\overline{C} = \frac{\bar{i}}{v} = \frac{\left[1/(V_2 - V_1)\right] \times \int_{V_1}^{V_2} i(V)\mathrm{d}V}{v} \tag{6}$$

where V_1 and V_2 (in V) are the switching potentials in CV, $\int_{V_1}^{V_2} i(V)\mathrm{d}V$ is the voltammetric charge obtained by integration of the positive or negative sweep in CV. The upper-limit potential $V_2 = V_1 + vt$ (t is the time period of a single positive or negative sweep). Therefore, eqn (6) becomes:[145,146]

$$\overline{C} = \frac{\int_{t_1}^{t_2} i(t)\mathrm{d}t}{V_2 - V_1} \tag{7}$$

The mass specific capacitance (C_s), is calculated from $C_s = C/m$, where m (in g) is the total mass of the active materials.

4.1.2 The GCD method. For the GCD method, the SC is charged to a desired voltage and discharged at a constant current until the voltage between the working electrode and the reference electrode (three-electrode cell) or the counter electrode (two-electrode cell) decreases to 0.0 V. The value for C_s can be deduced from the discharge curve according to:[145,146]

$$C_s = \frac{i}{|(\mathrm{d}V/\mathrm{d}t) \times m|} \tag{8}$$

where dV/dt (in V s^{-1}) is the slope of the discharge curve. Because the curve can be treated as a linear one, dV/dt is close to its mean value ($\Delta V/\Delta t$) where Δt (in s) is the time period for the overall potential decrease in a discharge curve. Then, eqn (8) can be approximated as:[145,146]

$$C_s = \frac{i \times \Delta t}{\Delta V \times m} = \frac{Q}{\Delta V \times m} \tag{9}$$

where Q (in C) is the overall charge released during the discharge process.

4.1.3 The EIS technique. The role of EIS is dependent on the ability to distinguish the contribution of each component of the electrochemical cell. Data recorded by EIS are modelled into an equivalent electrical circuit, which consists of circuit elements such as the resistance of the electrolyte (R_{sol}), the electrochemical double-layer capacitor produced from charge separation at the active materials/electrolyte interface (C_{dl}), and the bulk Faradaic impedance of the active materials. The bulk Faradaic impedance can be divided into pseudocapacitance (C_p) in parallel with a resistance which is the charge transfer resistance (R_{ct}) in a redox process.[145,147]

For a two-electrode SC, the two working electrodes are separated by a separator, and the potential difference of the two electrodes is monitored and controlled. Each electrode/electrolyte interface represents a capacitor and resistance. The overall capacitor is considered as two sub-capacitors in series. Therefore, the total capacitance (C_{total}), the capacitance per unit mass of the electrode materials, is calculated according to:[148]

$$\frac{1}{C_{total}} = \frac{1}{C_{s,1}} + \frac{1}{C_{s,2}} \quad (10)$$

where $C_{s,1}$ and $C_{s,2}$ (both in F g^{-1}) are the specific capacitances of the negative and positive electrodes, respectively.

In the literature, both three-electrode cells and two-electrode cells have been employed to evaluate the electrocapacitance of materials. Thus, the specific capacitance reported for similar electrode materials can be quite different. Thus is mainly due to the use of different electrode configurations (two-electrode and three-electrode configurations). Other factors such as fabrication of electrode thin films, current collectors and electrolytes used may also account for the inconsistency. The three-electrode specific capacitance, $C_{3\text{-}E}$ (in F g^{-1}), and the two-electrode specific capacitance, $C_{2\text{-}E}$ (in F g^{-1}), are related in eqn (11):[149]

$$C_{3\text{-}E} = 4C_{2\text{-}E} \quad (11)$$

In addition to the specific capacitance, energy and power densities are the two important parameters to evaluate the performance of a SC. The approach to obtaining the energy density and power density is based on the specific capacitance (C_{total}) of a two-electrode system. The maximum energy (E_{max}, in W h kg^{-1}) stored and power (P_{max}, in W kg^{-1}) delivered for a SC are calculated according to eqn (12) and (13), respectively:[145,148,150]

$$E_{max} = \frac{1}{2} C_{total} V^2 \quad (12)$$

$$P_{max} = V^2/4R_s \quad (13)$$

where V is the operating voltage, which is determined by the thermodynamic stability of the electrolyte and the electrodes. According to eqn (12) and (13), a high-performance SC must have a large capacitance, wide operating voltage, and minimum R_s (equivalent series resistance). The weight and volume of the cell should also be as low as possible for high-performance SCs.

4.2 Graphene-based electrodes for EDLCs

Graphene EDLCs were first explored by Ruoff and co-workers,[151] who used chemically modified graphene as the electrode. The specific capacitances in aqueous and organic electrolytes were about 135 and 99 F g^{-1}, respectively. A green route to reduce GO using urea as the reducing agent was developed by Lei and co-workers[152] to prepare graphene for SCs. Urea was found to be an effective reducing agent in removing oxygen-containing groups from GO for restoring the conjugated electronic structure. Capacitances as high as 255 and 100 F g^{-1} at current densities of 0.5 and 30 A g^{-1} respectively and a capacity retention of 93% were achieved. The performance is better than other graphene electrodes reduced by hydrazine (100–200 F g^{-1}), microwave reduction (100 F g^{-1}) and hydrothermal reduction (139 F g^{-1}). The superior performance of the urea-reduced graphene is ascribed to the porous network and partially restored π-conjugation structure, which facilitated fast ion and electron transports during the charge–discharge process (Fig. 8).

High-surface-area graphene has been produced using the chemical activation method.[153,154] Chemical activation of exfoliated GO can produce porous graphene with a BET surface area as high as 3100 m^2 g^{-1}, high electrical conductivity and low oxygen and hydrogen contents. A continuous, three-dimensional carbon network with atom-thick walls forms pores primarily 0.6–5 nm in width, greatly benefitting ion transport (Fig. 9). With an organic electrolyte, an energy density of 70 W h kg^{-1} was achieved at a current density of 5.7 A g^{-1} and working voltage of 3.5 V. Highly conductive and free-standing porous graphene films have also been prepared by chemical activation of GO for SCs.[16] After activation, the electrodes possessed a very high specific surface area of 2400 m^2 g^{-1} with a high in-plane electrical conductivity of 5880 S m^{-1}. A specific capacitance of 120 F g^{-1} and an energy density of 26 W h kg^{-1} were achieved.

Shi *et al.*[155] prepared a self-assembled graphene hydrogel *via* a one-step hydrothermal reduction process. The graphene hydrogel had 3D networks consisting of ultrathin graphene walls and cross-linking sites formed by regional π–π stacking of graphene sheets. The specific capacitances of the hydrogel

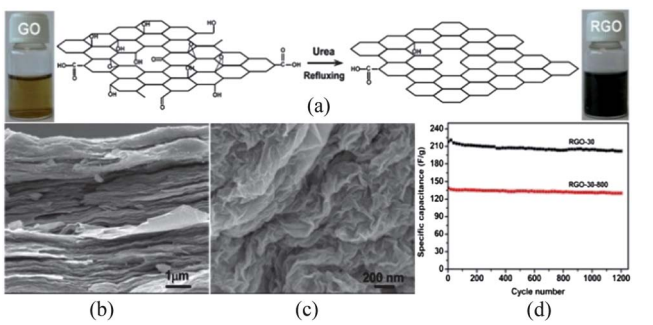

Fig. 8 (a) Scheme of the process of reducing GO using urea as the reducing agent; (b and c) SEM images of graphene by the above process; (d) cycle performance of graphene reduced by urea as the reducing agent. Reproduced with permission.[152]

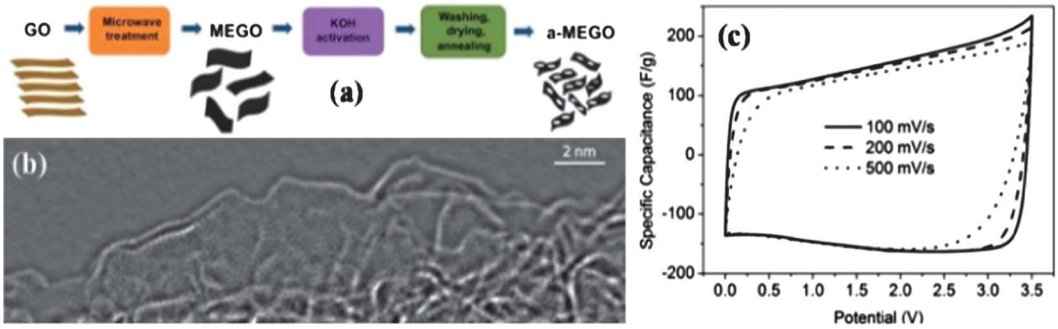

Fig. 9 (a) Scheme of the process for chemical activation of graphene; (b) HRTEM image of chemically activated graphene; (c) CV curves of chemically activated graphene at different scan rates. Reproduced with permission.[153]

electrodes at scan rates of 10 and 20 mV s^{-1} were calculated to be 175 and 152 F g^{-1}, which is about 50% higher than that of the SC based on graphene agglomerate particles tested under the same conditions. More importantly, this method can be extended to fabricate graphene composites with other nanomaterials for fabricating high-performance EDLCs or pseudocapacitors.

Pillaring graphene sheets with other materials is another approach to improving the electrochemical performance of graphene EDLCs. The open surface of graphene can hardly be fully utilized because graphene sheets tend to randomly aggregate during electrode preparation and fabrication, resulting in substantial loss in the active surface and generating a large number of discontinuous channels that retard ion transport, especially in aqueous solution due to the hydrophobic nature of graphene. Many reports have shown that separating graphene layers with nanosized carbon can greatly improve the electrochemical performance of the materials owing to the increase in the surface area and the opening of channels for ion transport.[156–160] Carbon black (CB) nanoparticles were used as spacers to avoid the self-restacking of graphene.[156] The CB–pillared graphene electrode exhibited an excellent electrochemical performance and cyclic stability compared with graphene electrode.

The preparation of 3D carbon based architectures consisting of graphene sheets with intercalated mesoporous carbon spheres (MCS) has been described by Lei and co-workers.[157] The preparation is schematically illustrated in Fig. 10a. A negatively charged GO colloid strongly interacts with positively charged mesoporous silica spheres, which are subsequently used as the template for replicating MCS *via* a chemical vapour deposition process, during which the GO was substantially reduced to RGO. Removal of the silica spheres leaves behind a 3D porous carbon architecture with RGO sheets intercalated by the MCS. The composite showed a substantially lower ESR and a higher power capability than the pure graphene electrode due to the larger surface area and the presence of pores for ion transport. The composite electrode also exhibited excellent electrochemical cyclability with 94% capacitance retention after 1000 cycles of charge–discharge (see Fig. 10b).

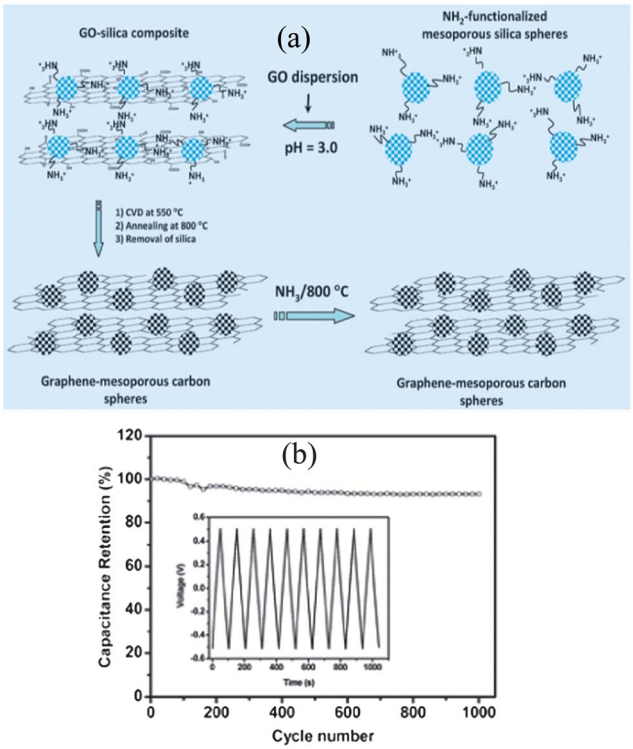

Fig. 10 (a) Schematic of preparing 3D mesoporous carbon spheres–graphene composites; (b) cyclability of the composites in 6 M KOH electrolyte. Reproduced with permission.[157]

The use of CNTs to separate graphene sheets has been demonstrated for preparing high-surface-area graphene electrodes.[158–162] Spin-coating and layer-by-layer assembly are the commonly used methods.[158–160] However, the hybrids thus prepared consist of aggregated graphene layers with relatively poor controllability. *In situ* growth of CNTs between graphene layers has been shown to be a very effective approach to pillaring graphene sheets.[161,162] Wei *et al.*[162] prepared 3D CNT/graphene nanostructures by *in situ* growth of CNTs between graphene sheets. The unique carbon structure endowed a high rate of ion and electron transports and comprehensive utilization of both pseudo and double-layer capacitances. A SC based

on this 3D CNT/graphene exhibited a specific capacitance of 385 F g^{-1} at 10 mV s^{-1}. After 2000 cycles, a capacitance increase of *ca.* 20% was observed due to the increased effective interfacial area.

4.3 Graphene-based electrode for pseudocapacitors

Pseudocapacitors store energy *via* Faradaic reactions occurring at the surface or near the surface of an electrode.[145] Compared with EDLCs, pseudo-capacitors have a higher specific capacitance, but usually show a lower operating voltage and a poorer cycling stability. In theory, any material with fast and reversible redox reactions can be used as an electrode material for pseudo-capacitors. Up to now, the most attractive materials for pseudo-capacitors are metal oxides/hydroxides and conducting polymers.[26] For metal oxides or hydroxides, the redox reactions can be attributed to the transition of two or more redox states of the metal cation. For conducting polymers, the redox reactions are caused by the transition of different doped and de-doped states.[26] However, the application of these pseudocapacitive electrode materials is largely limited by the following two factors. One is the low conductivity of de-doped conducting polymers and metal oxides/hydroxides. The other one lies in the fact that the electrochemical reaction often occurs at the surface of the electrode, resulting in ineffective utilization of the active material. In addition to these two factors, conducting polymers tend to have poor structure stability, leading to rapid aging of the polymer during electrochemical cycling.

4.3.1 Graphene–conducting-polymer composites. Conducting polymers have a characteristic structure with aromatic rings. Each carbon atom links with two adjacent carbon atoms by σ bonds to form the rings. The 2p orbitals of carbon atoms form delocalized π bonds at the vertical directions of the carbon planes. To date, the most widely used conducting polymers are polyaniline (PANi) and polypyrrole (PPy). Manthiram *et al.*[163] prepared PANi-coated graphene for SCs. The capacitance was measured to be as high as 408 F g^{-1}, which is about 4 times higher than that of graphene. Chemically modified graphene and PANi nanofiber composites were prepared by using an *in situ* polymerization method under acidic conditions (Fig. 11).[164] The obtained GO–PANi composites were reduced to graphene–PANi followed by reoxidation and reprotonation of the reduced PANi. SCs based on this graphene–PANi composite showed a specific capacitance of 480 F g^{-1} and a good cycling stability. The preparation of PPy nanosheets decorated on graphene was demonstrated.[165] Sheet-like PPy with a thickness of 20–50 nm grown on the surface of graphene/PPy polymerized at an early stage due to the dominated role of graphene and residual glucose in the synthesis process. Because of the larger surface area and short ion diffusion distance, ~95% of the capacitance was retained after 1000 cycles at a scan rate of 100 mV s^{-1}. Wei *et al.*[166] described the preparation of hierarchical nanocomposites by combining one-dimensional PANi nanowires with GO. The PANi nanowire arrays aligned vertically on the GO surface. Capacitances of 555 and 227 F g^{-1} were obtained at current densities of 0.2 and 2 A g^{-1}, respectively. Interestingly, the GO–PANi composite exhibited a much higher stability than randomly connected PANi nanowires. For instance, after 2000 cycles, the capacitance retention of the composite was still 92% of its initial capacitance, while the pristine PANi retained only 74%.

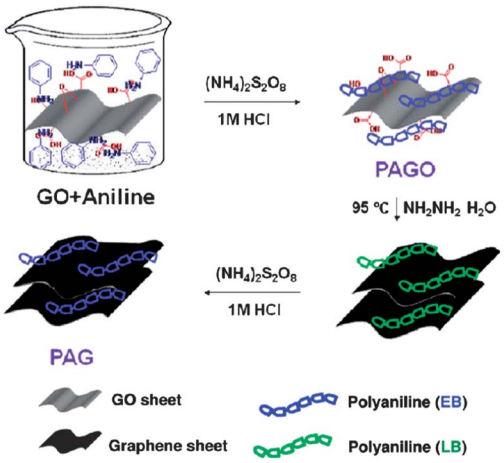

Fig. 11 Illustration of the process of preparing graphene–PANi composites. Reproduced with permission.[164]

Composite films consisting of graphene and PANi nanofibers with a sandwiched layer structure were prepared by using the vacuum filtration method.[167] A SC based on the composite films showed an electrochemical capacitance of 210 F g^{-1} at 0.3 A g^{-1}. Flexible graphene/PANi and sulfonated graphene/PPy films fabricated using the electrochemical polymerization method exhibited specific capacitances of 233 and 285 F g^{-1}, respectively.[168,169]

4.3.2 Graphene–metal oxide/hydroxide composites. RuO_2, especially hydrous and amorphous RuO_2, is one of the most promising electrode materials for SCs due to its high specific capacitance, highly reversible redox reactions in a wide potential range and long cycle life.[170,171] Ren and co-workers[172] prepared hydrous RuO_2–graphene composites with different loadings of Ru. The composites exhibited a capacitance of 570 F g^{-1} at a 38.3 wt% Ru loading, enhanced rate capability, excellent electrochemical stability (97.9% retention after 1000 cycles), and a high energy density (20.1 W h kg^{-1}). The composite electrode performed electrocapacitively much better than both pure RuO_2 and pure graphene electrodes. In spite of the excellent performance, the high cost of RuO_2 greatly restricts its commercial applications.

MnO_2 is a very promising material for pseudo-capacitors because of its rapid redox reaction, wide operating voltage, low-cost, stability and environmental friendliness.[173–175] The direct reaction of graphene with $KMnO_4$ is the most commonly used method for preparing graphene–MnO_2 composites.[176,177] The redox reaction is shown below:

$$4MnO_4^- + 3C + H_2O \rightleftarrows 4MnO_2 + CO_3^{2-} + 2HCO_3^- \quad (14)$$

In this reaction, the carbon substrate serves as a sacrificial reductant and converts aqueous permanganate to insoluble MnO_2, which deposits on the surface of graphene. An asymmetric electrochemical capacitor fabricated with a

graphene–MnO_2 composite as the positive electrode and activated carbon fibres (ACF) as the negative electrode exhibited an energy density as high as 51.1 W h kg^{-1} (about five times higher than that of AC-based symmetric SCs) (see Fig. 12),[176] and the device can be cycled reversibly in the voltage range of 0–1.8 V retaining 97.3% of the initial capacitance after 1000 cycles. The interface assembly method has been used to prepare MnO_2–graphene composites.[178,179] Cheng *et al.*[179] demonstrated an asymmetric supercapacitor with graphene as the negative electrode and MnO_2 nanowire–graphene composite prepared by using the interface assembly method as the positive electrode in a neutral aqueous electrolyte. The capacitor device can be charged/discharged at voltages up to 2.0 V. Other metal oxides, such as NiO, Co_3O_4, RuO_2 have also been studied as electrode materials for SCs.[172,180–184] Chen *et al.*[184] used a simple hydrothermal procedure to synthesize Co_3O_4 nanowires on 3D graphene foam as electrode materials for SCs. The 3D graphene–Co_3O_4 composite could deliver a specific capacitance of ~1100 F g^{-1} at a current density of 10 A g^{-1} with an excellent stability.

Metal hydroxides, such as $Co(OH)_2$, $Ni(OH)_2$ and double layer hydroxides (DLHs), have been combined with graphene to make composite electrode materials for SCs.[185–192] Dai and co-workers[188] described an *in situ* growth method for preparing single crystalline $Ni(OH)_2$ nanoplates on graphene. A specific capacitance of 1335 F g^{-1} was observed at a current density of 2.8 A g^{-1}. At a very high current density, 45.7 A g^{-1}, the capacitance was as high as 953 F g^{-1}. Characterization data showed that the conductivity of the graphene was very high and the $Ni(OH)_2$ nanoplate was very thin (about ~10 nm). A composite material consisting of flowerlike $Ni(OH)_2$ particles and graphene sheets has been prepared by using a facile and cost effective microwave assisted method.[186] An asymmetric capacitor cell fabricated with flowerlike $Ni(OH)_2$/graphene as the positive electrode and graphene as the negative electrode displayed a specific capacitance of 218.4 F g^{-1} and an energy density of 77.8 W h kg^{-1}. The specific capacitance was 94.3% after 3000 cycles. The outstanding electrocapacitive performance was attributed to the synergistic effect of both components and the very short diffusion length of the flowerlike structure.

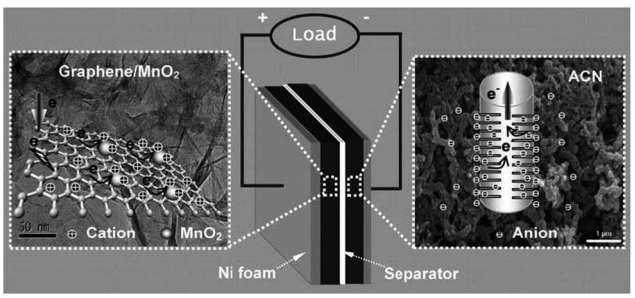

Fig. 12 Schematic illustration of the fabricated asymmetric supercapacitor device based on a graphene–MnO_2 composite as the positive electrode and activated carbon nanofibers as the negative electrode. Reproduced with permission.[176]

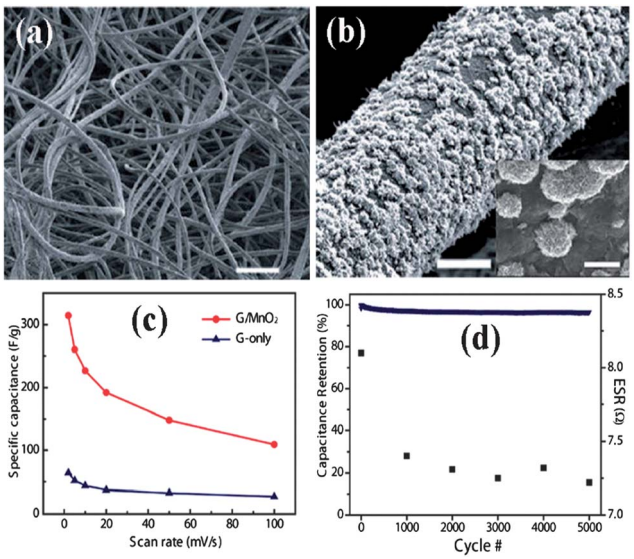

Fig. 13 (a) SEM image of a sheet of graphene-coated textile after 60 min MnO_2 electrodeposition, scale bar is 200 μm; (b) SEM image of a microfiber coating of MnO_2 nanostructures, the inset is a high magnification SEM image showing flowerlike MnO_2 nanostructures, scale bars are 5 and 1 μm; (c) comparison of specific capacitance values of the hybrids and graphene at different scan rates; (d) cycling performance of the AECs. Reproduced with permission.[202]

4.4 Flexible electrodes for SCs

Portable electronic devices that are small, thin, light, and flexible are highly desirable.[193–195] Graphene has been studied as a flexible electrode for SCs and LIBs.[18,196,197] Pure graphene films were shown to display a low specific capacitance.[198,199] A graphene–cellulose paper (GCP) SC exhibited a specific capacitance of only about 120 F g^{-1}.[199] Chemically modified graphene and graphene-based composites with pseudocapacitive materials have been studied to improve electrochemical properties.[154,167,168,183,200,201] For example, Cui and co-workers[202] applied the electrodeposition technique to decorate graphene-coated 3D porous textile with MnO_2 particles (Fig. 13a and b). The specific capacitance is as high as 315 F g^{-1}, much superior to that of graphene only. And ~95% of the capacitance is retained over 5000 cycles (Fig. 13c and d). Multilayer films of Co–Al layered double hydroxides on graphene were fabricated through the LBL assembly technique and exhibited a high capacitance of 1204 F g^{-1} and 90 F cm^{-2} with good stability over 2000 cycles.[201]

5 Graphene-based electrodes for LIBs

In comparison with SCs, LIBs possess the advantages of high specific energy, high efficiency and low cost.[203] As schematically illustrated in Fig. 14, a LIB typically consists of a positive electrode (cathode), a negative electrode (anode), a porous membrane (allowing lithium ions to travel through) separating the two electrodes, and an electrolyte (playing the role of conducting lithium ions during charge and discharge). They have become one of the main power sources for small portable appliances in modern society, such as mobile phones, digital cameras and laptop computers. However, the current LIBs

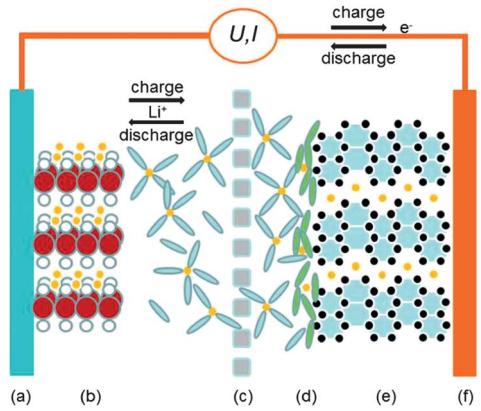

Fig. 14 Schematic illustration of a LIB cell: (a) aluminum current collector; (b) cathode; (c) porous separator; (d) solid electrolyte interface layer; (e) graphite anode; (f) copper current collector.

cannot satisfy the intensively increasing needs from massive power-storage devices used in, for examples, electric vehicles and grid power management. Electrodes play a paramount role in the development of high-performance batteries. Research efforts have thus been largely put on improving current electrode materials or exploring new electrode materials.

5.1 The working principle of LIBs

A typical LIB can be represented below:

$$(-)\ C_n|1\ \text{mol}\ L^{-1}\ LiPF_6\text{–}EC + DEC|LiMO_x\ (+) \quad (15)$$

where C stands for a carbonaceous material and M indicates a metal. On the cathode, the following reaction occurs:

$$LiMO_x - ye^- \underset{\text{discharge}}{\overset{\text{charge}}{\rightleftharpoons}} Li_{1-y}MO_x + yLi^+ \quad (16)$$

while on the anode, the following reaction takes place:

$$C_n + yLi^+ + ye^- \underset{\text{discharge}}{\overset{\text{charge}}{\rightleftharpoons}} Li_yC_n \quad (17)$$

The overall reaction becomes:

$$LiMO_x + C_n \underset{\text{discharge}}{\overset{\text{charge}}{\rightleftharpoons}} Li_{1-y}MO_x + Li_yC_n \quad (18)$$

During the charging process, lithium ions are deintercalated from the cathode into the electrolyte, diffuse across the porous separator, and intercalate into the carbonaceous anode. During the discharging process, the lithium ions are deintercalated from the anode and intercalate back to the empty sites between layers of the cathode. Therefore, such a LIB is called a "rocking chair" battery because of the lithium ion transfer mechanism.

The battery capacity is defined as the amount of charge that can be obtained *via* the charging and discharging processes under specific conditions. The theoretical capacity of a battery determined by the amount of an active material is given by:[204]

$$C_o = 26.8n\frac{m_o}{M} = \frac{1}{q}m_o(\text{A h}) \quad (19)$$

where C_o in A h is the theoretical capacity, m_o in g is the mass of the active material participating in the electrochemical reaction, M in g mol^{-1} is the molar weight of the active material, n is the number of electrons involved in the reaction, and q is the electrochemical equivalence. For example, the theoretical capacity of a graphite anode with six coordinated carbon atoms for each Li ion (LiC_6) is calculated as below:[204]

$$LiC_6 \rightarrow Li^+ + C_6 + e \quad (20)$$

$$LiC_6 = 26.8 \times \frac{1}{78.94} \times 1000 = 339.50\ (\text{mA h g}^{-1}) \quad (21)$$

The actual capacity of a battery at constant current is given by:

$$C = it \quad (22)$$

or

$$C = \frac{1}{R}\int_{t_1}^{t_2} V\,dt \quad (23)$$

The theoretical energy value of a battery is the maximum value that can be delivered:

$$W_o = C_oV_o \quad (24)$$

where V_o is the standard potential (in V).

According to eqn (20), the maximum power that can be produced by the battery is given by:

$$P_o = iV_o \quad (25)$$

The actual energy and power are determined by substituting the working voltage into eqn (20) and (21), respectively.[204]

Similar to SCs, CV, GCD and EIS are the common methods to test the performance of lithium ion batteries.

5.2 Graphene-based anodes

Graphite with a theoretical capacity of 372 mA h g^{-1} on the basis of the fact that one Li ion interacts with six carbon atoms is the most commonly used anode in LIBs because of its excellent reversible capacity for Li ions and long cycling life.[205] In theory, graphene can accommodate Li ions on both sides. This makes the theoretical capacity two times larger than that of other carbon materials, such as carbon nanotubes (CNT). Theoretical calculations showed that graphene possesses a maximum capacity of 740 mA h g^{-1} on the basis of double-layer adsorption configuration.[206] Sato and co-workers[207] used the ^{7}Li nuclear magnetic resonance (NMR) technique to study the transport mechanism in disordered carbon, and proposed a model of Li_2 covalent molecule configuration that a Li_2 molecule is loosely trapped by two adjacent benzene rings in the carbon. The most saturated Li storage state can be LiC_2 to give a capacity of up to 1116 mA h g^{-1}. Both configurations suggest a higher capacity of graphene anode. Another study[208] showed that graphene and graphite have a similar interaction model with Li ions. However,

because of the repulsion forces between Li^+ at both surfaces of graphene, the amount of adsorbed Li ions on single-layered graphene is lower than the theoretically predicted value. Uthaisar and Barone[209] studied the edge effects of Li diffusion in graphene by means of density functional theory and showed that narrower graphene nano-ribbons, especially with a zigzag morphology, can provide a faster discharge rate owing to the lowering of energy barriers and diffusion length.

Apart from the nice theoretical studies, experimental investigation has been carried out to investigate graphene anode for LIBs. Guo *et al.*[210] prepared crumpled-paper-shaped graphene nanosheets by means of oxidation, rapid thermal expansion, and ultrasonic treatment of graphite. The electrochemical performances of the prepared graphene nanosheets were compared with that of the graphite. A capacity of 672 mA h g^{-1} with superior cycling stability was observed from the graphene anode. However, no obvious plateau was observed from the charge–discharge curves of the graphene nanosheets while a voltage at ~0.2 V in each charge process of the artificial graphite anode could be clearly seen. The authors attributed the observation of the absence of a plateau of the graphene anode to its small crystallite, high surface area, and disordered stacking of graphene sheets. Lian and co-workers[211] used the thermal exfoliation method to prepare curled, few-layered graphene. The reversible specific capacity of the first cycle was as high as 1264 mA h g^{-1} at a current density of 100 mA g^{-1}. The capacity became 848 mA h g^{-1} after 40 cycles at the same current density. The high capacity might be attributed to the large surface area, curled morphology as well as the presence of hydrogen on the graphene. However, there was again no clear voltage plateau on the charge and discharge curves. A flower-petal shaped RGO anode exhibited a discharge capacity of 945 mA h g^{-1} and charge capacity of 650 mA h g^{-1}. A specific capacity of 460 mA h g^{-1} was obtained after 100 cycles, indicating an excellent cycling stability. The double-layer adsorption model was believed to function in addition to the Li ion storage by the nano-cavities formed between graphene sheets.[212]

Yoo and co-workers[213] used CNT and fullerene (C_{60}) as the spacer between graphene layers to prepare high-surface-area anode materials. Improvement in specific capacity upon adding CNT and C_{60} was achieved. However, the CNT- or C_{60}-modified graphene anodes did not show an obvious potential plateau due to disordered stacking of the graphene sheets. Zhao *et al.*[214] prepared flexible holey graphene using the mechanical cavitation–chemical oxidation method. The cycling performance showed that the highest reversible capacity was below 300 mA h g^{-1} although the electrode was stable after 400 cycles. One-dimensional graphene nanoribbons prepared by unzipping pristine multiwalled carbon nanotubes were used as the anode for LIBs.[215] Interestingly, the sample before reduction exhibited a higher specific capacity than the sample after reduction. The residual oxygen species enhanced the formation of a more stable Li-rich solid electrolyte interface (SEI). There was a capacity loss of about 3% per cycle.

While improvements have been achieved by employing graphene as an anode material for LIBs, great challenges still remain. A key challenge is the fast capacity loss in the first few cycles due to the formation of the SEI layer. The fact that a graphene anode does not exhibit a clear stable voltage plateau indicates that graphene-based batteries may fail to provide a stable voltage output.

5.3 Graphene-based composites as anodes

5.3.1 Graphene–Si composites. Silicon (Si) that is regarded as one of the most promising anode materials for next-generation LIBs possesses the highest theoretical capacity (4200 mA h g^{-1}) and low discharge potential.[216] The key issue with a Si anode is its extremely poor cycling stability due to severe volume change (about 300%) during the lithiation and delithiation processes.[217]

Chou and co-workers[218] prepared a Si–graphene composite anode by mixing commercial Si nanoparticles with graphene. The electrode exhibited a specific capacity of 1168 mA h g^{-1} after 30 cycles with a coulombic efficiency of 93% on average. Impedance spectroscopy data showed that the charge-transfer resistance of the composite anode was less than half of that of Si nanoparticles. Besides, the flexibility of the composite accommodated large inner strains and high surface area and the porous structure contributed to the penetration of the electrolyte. On the other hand, the persistent capacity fading was attributed to the contacting of Si and the electrolyte, as well as the pulverization of Si particles. Tao *et al.*[217] studied self-supporting Si–RGO nanocomposite films prepared simply by filtering a Si/GO suspension followed by thermal reduction under Ar atmosphere. The reversible specific capacity in the first cycle was 1040 mA h g^{-1}. The capacity became 786 mA h g^{-1} after 300 cycles at a current rate of 50 mA g^{-1}. However, the rate capacity decreased significantly as the current rate increased from 50 to 5000 mA g^{-1}.

Thermal reduction of a Si–GO composite was found to lead to partial restacking of graphene to form graphite (Fig. 15).[219] Specific capacities of 2200 and 1500 mA h g^{-1} were obtained after 50 and 200 cycles, respectively. The reconstitution of graphene improved the electron conductivity of the 3D network anode as well as a better connection with Si nanoparticles. It was also pointed out that excessive constitution of graphene sheets should be avoided to allow Si nanoparticles to disperse homogeneously in the composite. Thermally reduced GO and thermally expanded graphite were used to prepare Si–graphene composite anodes.[220] The composite prepared using the thermally expanded graphite showed a higher initial specific

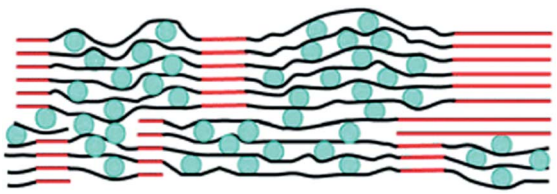

Fig. 15 Cross-sectional schematic drawing (not to scale) of a high-capacity, stable electrode, made of a continuous, conducting 3-D network of graphite (red) anchoring regions of the graphene–Si composite. Blue circles: Si nanoparticles, black lines: graphene nanosheets. Reproduced with permission.[219]

capacity. Zhou *et al.*[221] prepared Si–graphene composites using thermally reduced GO and observed a significantly improved cycling performance – a specific capacity of 1153 mA h g^{-1} was observed after 100 cycles. To create good structural integrity and electronic conduction between Si nanoparticles and graphene matrix, aromatic linkers through diazonium chemistry were used to form covalent bonds. The novel Si–phenyl–graphene nanocomposites exhibited a specific capacity of 1079 mA h g^{-1} during the first delithiation process and a specific capacity of 828 mA h g^{-1} could be retained after 50 cycles.[222]

In addition to Si nanoparticles, 1D Si nanowires have been studied as well. Wang and Han[223] prepared a Si porous nanowire/graphene electrode as the anode, which showed an initial specific charge capacity of 2347 mA h g^{-1}. After 20 cycles, the capacity still remained 2041 mA h g^{-1}. The remarkable performance of the composite anode was attributed to the excellent charge conductivity of graphene nanosheets as well as the porous structure of 1D Si nanowires. In another study,[224] the vapour deposition method was employed to synthesize uniformly deposited continuous Si films on the graphene surface. The as-prepared anode delivered a stable specific reversible capacity of about 1060 mA h g^{-1} for 150 cycles at a current density of 1400 mA g^{-1}. Zhao *et al.*[225] prepared a vacancy-enabled high-power Si–graphene composite anode using a facile wet chemical method. The anode showed a reversible capacity of 3200 mA h g^{-1} after 5 cycles at 1000 mA g^{-1}, which was close to the theoretical value. After 150 cycles, about 83% of its theoretical capacity was maintained with a capacity loss of only 0.14% per cycle. When cycled at 4000 mA g^{-1} (about 1.3 C), the capacity was about 600 mA h g^{-1}.

5.3.2 Graphene–Sn/SnO_2 composites. Sn and SnO_2 are promising anode materials with high theoretical capacity. The reversible capacity of Sn is as high as 994 mA h g^{-1} when the alloy $Li_{4.4}Sn$ forms during lithiation and the theoretical capacity of SnO_2 is 782 mA h g^{-1}.[226,227] However both Sn and SnO_2 suffer from a severe volume change during cycling.[228,229] Sn nanoparticle–graphene composites with a 3D architecture were prepared *via* chemical reduction of both GO and Sn^{2+} in an aqueous solution.[226] The prepared composite anode exhibited an initial discharging capacity of 1250 mA h g^{-1} and a reversible charging capacity of 810 mA h g^{-1}. The formation of SEI was the primary reason for the capacity loss. It could maintain a capacity of 508 mA h g^{-1} after 100 cycles with a coulombic efficiency of 96.5%. It was believed that graphene in the composite could not only contribute to the general capacity of the electrode but also create voids between them to efficiently buffer the volume change during cycling.

Ji and co-workers[230] described a 3D multilayered nanostructure consisting of Sn nanopillars and graphene as is seen from the SEM images in Fig. 16. Sn nanopillar arrays were embedded between graphene sheets using a conventional film deposition method. The composite anode showed an initial specific charge and discharge capacities of 945 and 734 mA h g^{-1}, respectively. The capacity loss was ascribed to the formation of SEI on the surface of the electrode. After the 15th and 30th cycles, the capacities were 723 and 679 mA h g^{-1}, respectively, indicating a slow capacity fading. The material also exhibited an improved rate capacity as expected. The capacities remained 508 mA h g^{-1} after 40 cycles at a current rate of 500 mA g^{-1}, 501 mA h g^{-1} after 30 cycles at 1000 mA g^{-1}, and 408 mA h g^{-1} after 35 cycles at 5000 mA g^{-1}. The 3D structure provided space to accommodate volume change and alleviated the inner stress/strain during lithiation/delithiation. Besides, the Sn nanopillars enhanced the penetration rate of Li ions between neighbouring nanopillars and reduced internal resistance. Graphene possesses the ability of storing Li; on the other hand, it could also enhance the electronic conductivity.

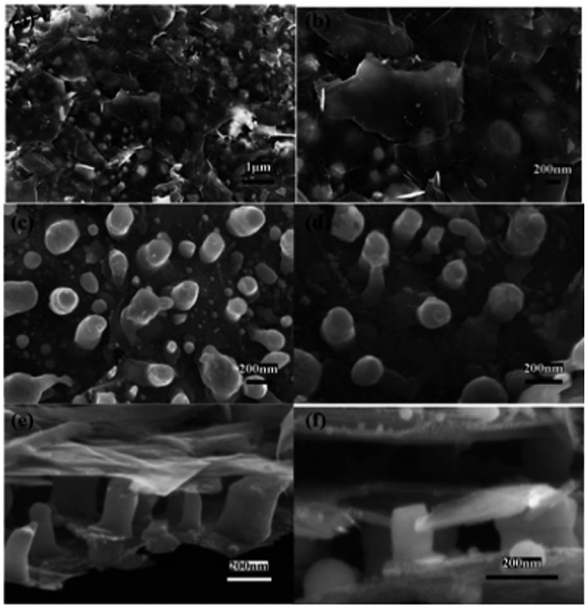

Fig. 16 SEM images of (a and b) top-views of the graphene/Sn-nanopillar nanostructures; (c and d) top-views of the Sn-nanopillar on graphene surfaces (after removal of the top graphene layers); (e and f) cross-sectional views of the graphene/Sn-nanopillar/graphene nanostructures. Reproduced with permission.[230]

Wen *et al.*[231] described the preparation of SnO_2-decorated graphene materials. SnO_2 nanoparticles and polymer films simultaneously grew on GO sheets. Different annealing temperatures (250, 550, 750, and 900 °C) were studied, and it was found that a SnO_x/C/graphene sample annealed at 550 °C showed the most remarkable improvement, delivering a capacity of 565 mA h g^{-1} after 30 cycles and displayed a much lower charge transfer resistance. Du *et al.*[228] prepared SnO_2–graphene nanocomposites *via* an *in situ* chemical synthesis method. The as-prepared composite exhibited a reversible capacity of 665 mA h g^{-1} after 50 cycles. Yao and co-workers[232] prepared similar materials and observed a reversible capacity of 765 mA h g^{-1} in the first cycle with an enhanced cyclability. Paek *et al.*[233] explored SnO_2/graphene nanoporous electrodes with a 3D delaminated flexible structure. The cycling performance was enhanced with a reversible capacity of 810 mA h g^{-1} and the charge capacity remained 570 mA h g^{-1} after 30 cycles. In comparison, the second charge capacity of bare SnO_2 nanoparticles was 550 mA h g^{-1} and decreased to 60 mA h g^{-1} after 15 cycles.

Zhang *et al.*[234] described a two-step method (Fig. 17) to load SnO_2 nanocrystals on both sides of single layer GO sheets. Sn^{4+} can selectively bond with oxygenated groups on the surface of GO. The initial specific capacity of the SnO_2–graphene composite was 786 mA h g^{-1}. After 50 cycles, there was about a 29% capacity loss. Xu and co-workers[235,236] described a one-step hydrothermal method to prepare hybrid materials of SnO_2 nanorods decorated on graphene. The material exhibited a discharge capacity as high as 803 mA h g^{-1} after 100 cycles. The space between the particles on the graphene, the nanometre size of the SnO_2, elastic graphene, formation of the uniform SEI all contributed to the observed good cycling performance.

5.3.3 Other graphene–metal-oxide composites. Apart from SnO_2, other metal oxides such as Co_3O_4, TiO_2, NiO and Fe_3O_4 have also been studied.[237–241] These metal oxides also suffer from severe aggregation and rapid capacity fading due to dramatic volume expansion.[242]

Wu and co-workers[237] reported an approach to preparing Co_3O_4-spaced graphene, in which Co_3O_4 nanoparticles worked as a spacer to separate graphene sheets. The composite exhibited a large reversible capacity of ~935 mA h g^{-1} after 30 cycles, an excellent coulombic efficiency of 98%, and a good rate capacity. Similar work performed by Kim *et al.*[243] showed reversible capacities of 990 mA h g^{-1} for the first cycle and 778 mA h g^{-1} for the 42nd cycle. The rate capacity was about 600 mA h g^{-1} at a current rate of 1000 mA g^{-1}. A one-step -solvothermal method was employed to synthesize Co_3O_4 nanorods–graphene nanocomposites. The obtained anode material showed an improved electrochemical performance (Fig. 18). The first discharge and charge capacities were 1303 and 917 mA h g^{-1}, higher than pure Co_3O_4 (1184 and 854 mA h g^{-1}, respectively). The composite anode still retained a capacity of 1310 mA h g^{-1} at the 40th cycle, a sharp comparison with 85 mA h g^{-1} for the pure Co_3O_4 anode at the 40th cycle. The pure graphene anode exhibited a lower initial efficiency of 40.6% and no obvious voltage plateaus. It was noticed that there was a slight increase in the reversible capacity with the increase of the cycling number due to the gradual activation of the nanocomposites.[244] Li and co-workers[245] described a Co_3O_4–graphene composite, which displayed a discharge capacity of 941 mA h g^{-1} in the 2nd cycle and 740 mA h g^{-1} in the 60th cycle at a current rate of 0.2 C. Co_3O_4–graphene nanoporous composite materials prepared by using the microwave irradiation method showed a rate capacity of 931 mA h g^{-1} at a current rate of 5 C. The capacity is larger than that of the theoretical value of pure Co_3O_4 (890 mA h g^{-1}), which was ascribed to the presence of nanocavities in the composite.[246]

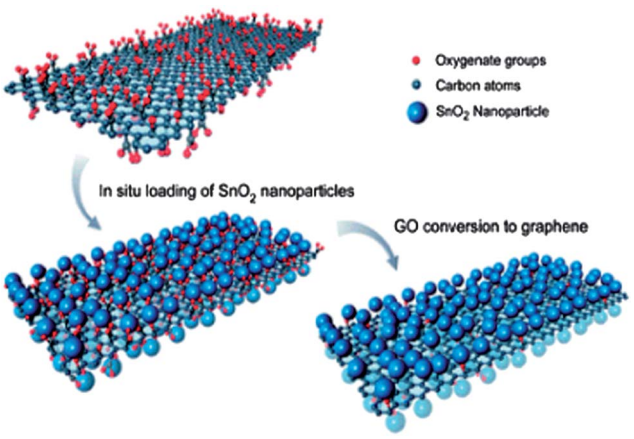

Fig. 17 A two-step method to load SnO_2 nanoparticles on both sides of single layer graphene sheets to form a SnO_2–graphene composite. Reproduced with permission.[234]

TiO_2 being environmentally friendly, cost-effective and stable against various environments has been mixed with functionalized graphene sheets to prepare LIB anode materials with an enhanced electrochemical performance at high charge–discharge rates.[238] Qiu *et al.*[247] used three steps to prepare TiO_2–graphene composites. Size-tuneable anatase TiO_2 nanospindles were first synthesized using the hydrothermal synthesis method with tubular titanate as a precursor. Then, TiO_2 nanospindles were dispersed on GO *via* a spontaneous self-assembly process. Finally, the nanocomposite was annealed in NH_3. The obtained anatase@oxynitride/titanium nitride–graphene hybrid composites anode showed excellent rate capacity and cycling performance compared with pure TiO_2. Directly grown ultrathin anatase TiO_2 nanosheets on graphene were reported to deliver discharge capacities of 285 and 213 mA h g^{-1} in the first and second cycles at a current rate of 1 C, respectively.[248]

NiO has attracted extensive attention as an anode material due to its high theoretical capacity (718 mA h g^{-1}), nontoxicity and low cost.[249,250] A liquid phase deposition method was used to prepare a NiO–graphene composite. It displayed a stable specific reversible capacity of 646.1 mA h g^{-1} after 35 cycles at a current density of 100 mA g^{-1}. When the current rates were increased to 400 and 800 mA g^{-1}, the capacities were measured to be 509 and 368.5 mA h g^{-1}, respectively, indicating a very good rate capacity of the material.[251] Homogeneous co-precipitation followed by annealing was used to prepare a NiO–RGO composite anode with capacities of 1040 mA h g^{-1} after 50 cycles at 100 mA g^{-1} and 727 mA h g^{-1} at 1600 mA g^{-1}.[252] Tao and co-workers[253] reported a 3D hierarchical NiO–graphene composite, which exhibited a high reversible capacity of about 1065 mA h g^{-1} after 50 cycles at a current density of 200 mA g^{-1}, which was ascribed to the buffering effect and the improvement of the electronic conductivity of composites.

Graphene was also employed to improve the performance of Fe_3O_4 *via in situ* reduction of iron hydroxide.[240] The graphene–Fe_3O_4 composite exhibited a reversible specific capacity of about 1026 mA h g^{-1} after 30 cycles at 35 mA g^{-1} and 580 mA h g^{-1} after 100 cycles at 700 mA g^{-1} as well as enhanced cycling stability and rate capacity. Lian *et al.*[254] prepared an Fe_3O_4–graphene nanocomposite *via* a gas/liquid interface reaction method. The prepared anode with 22.7 wt% graphene showed a stable reversible specific capacity of above 1000 mA h g^{-1} after 40 cycles at 100 mA g^{-1}, significantly outperforming Fe_3O_4 nanoparticles, which had a capacity value of 226 mA h g^{-1} after 34 cycles. The rate capacities of the anode were 740, 600, 410 mA h g^{-1} at current densities of 300, 500, 1000 mA g^{-1}, respectively. Graphene played an important part in preventing the Fe_3O_4 nanoparticles from aggregation and volume

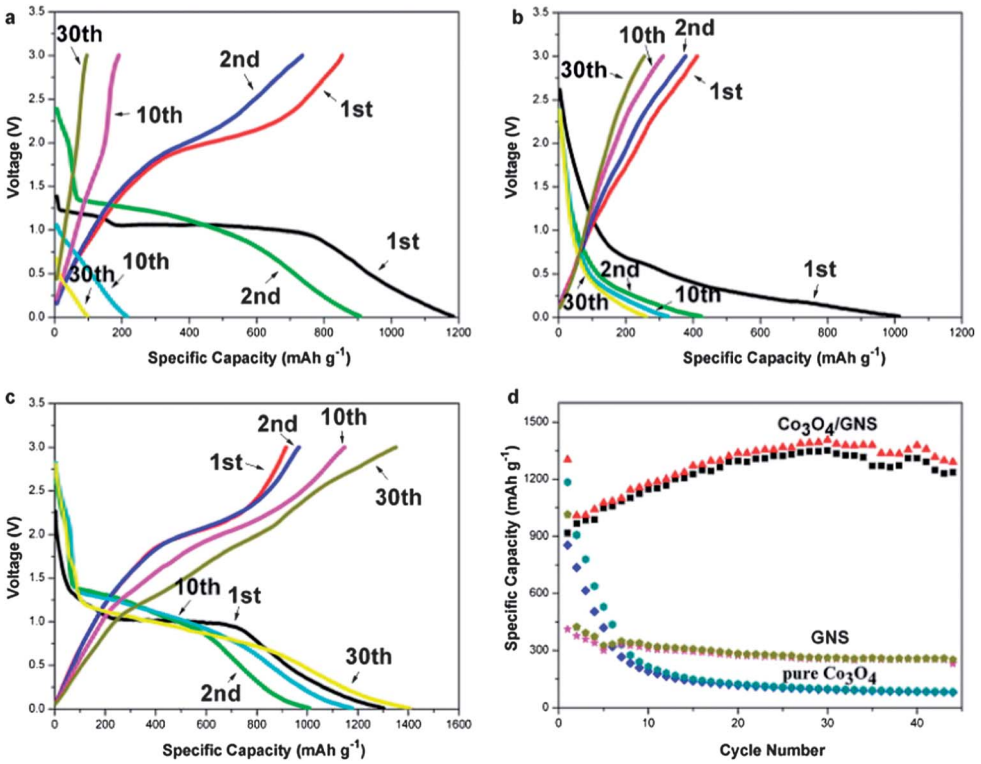

Fig. 18 Typical charge–discharge curves of (a) pure Co_3O_4, (b) graphene and (c) Co_3O_4 nanorods–graphene nanocomposites cycled at the 1st, 2nd, 10th and 30th between 0.01 V and 3.0 V. (d) The comparison of the cycling performance of pure Co_3O_4, graphene and Co_3O_4 nanorods–GNS nanocomposites. Reproduced with permission.[244]

expansion during cycling. In other research, microwave irradiation was used to synthesize an Fe_3O_4–graphene composite anode and it showed an initial discharge capacity of 1320 mA h g^{-1} and could still maintain 650 mA h g^{-1} after 50 cycles at C/10. The prepared anode could also exhibit high rate capacity (350 mA h g^{-1} at 5 C).[255] Chen and co-workers[256] designed graphene-encapsulated hollow Fe_3O_4 nanoparticles using a simple self-assembly process. The as-prepared anode exhibited a stable high specific reversible capacity of about 900 mA h g^{-1} over 50 cycles and 832 mA h g^{-1} at 100 mA g^{-1} after 90 cycles of charge and discharge. An Fe_3O_4–C–RGO composite was designed using the hydrothermal treatment method. The composite showed an initial specific discharge capacity of 952 mA h g^{-1} at 0.2 C. After 100 cycles, the capacity was 842 mA h g^{-1}. The improved performance was attributed to the presence of both the carbon shells and the RGO sheets, which enhanced electric conductivity and superior structure stability.[257] Zhou *et al.*[258] explored in-depth the interfacial interaction between Fe_3O_4 nanoparticles and graphene and the prepared Fe_3O_4–graphene composite as the anode material by direct pyrolysis of $Fe(NO_3)_3$ on graphene. Strong covalent bonds (Fe–O–C bond) with graphene measured by Fourier transform infrared (FTIR) spectroscopy enhanced the cycling stability of the electrode at a high current rate. It delivered a high capacity of 796 mA h g^{-1} after up to 200 cycles even without any capacity loss during cycling at a current density of 500 mA g^{-1} (about 0.6 C). It could also display a reversible capacity of about 550 mA h g^{-1} after 300 cycles at 1000 mA g^{-1} (about 1.3 C). By contrast, the electrodes made from mechanical mixing of a Fe_3O_4–graphene hybrid composite, pure graphene and Fe_3O_4 did not exhibit impressive performances under the same conditions. In recent research, a Fe_3O_4–graphene composite was prepared by a simple ultrasonic method and the composite anode exhibited significant electrochemical improvements, 1235 mA h g^{-1} after 50 cycles at 200 mA g^{-1}, 315 mA h g^{-1} at 10 000 mA g^{-1} and 450 mA h g^{-1} after 700 cycles at 5000 mA g^{-1}. The rate capacity and cycling stability were both enhanced remarkably.[259]

In summary, composite materials consisting of graphene sheets and metal oxide nanoparticles of various compositions and structures have been demonstrated to display significantly improved electrochemical performance compared with the pure metal oxide component or graphene. In comparison with CNTs, graphene has a larger specific surface area and is easy to combine with other materials.[260] Importantly, graphene-based composites exhibit superior lithium storage properties than CNT-based composites do.[235,236,238,247,261,262] The presence of graphene in the composite plays a number of roles, such as preventing the nanosized active particles from aggregation (thus maintaining the contact surface of the metal oxide for lithium ions), efficiently buffering the volume expansion and contraction of the particles during cycling, enhancing the rate capability because of its excellent electric conductivity, and reversibly storing lithium ions. On the other hand, the composite also benefits from the particles, which could act as spacers between graphene sheets enabling a highly accessible surface.

5.4 Graphene-based composites as cathodes

The olivine-type of $LiFePO_4$ with a theoretical capacity of 170 mA h g^{-1} (ref. 263 and 264) has been considered as a promising cathode material for LIBs. The main drawbacks of $LiFePO_4$ are the poor conductivity resulting from the low Li ion diffusion rate and low electronic conductivity.[265] In order to enhance the electronic conductivity of $LiFePO_4$, graphene has been used to modify $LiFePO_4$. Ding *et al.*[266] prepared a $LiFePO_4$–graphene composite *via* a co-precipitation method. Graphene played the role of scaffolds. The prepared cathode material with only 1.5 wt % graphene showed an initial discharge capacity of 160 mA h g^{-1} at 0.2 C and the capacity was maintained at 110 mA h g^{-1} at a higher rate (10 C). $LiFePO_4$–graphene composites were also prepared by a solid-state reaction and the composites exhibited an initial discharge capacity of 161 mA h g^{-1} at 0.1 C and a capacity of 70 mA h g^{-1} was still retained at a high rate of 50 C.[267] Su and co-workers[268] explored a novel $LiFePO_4$–graphene–carbon composite cathode material using an *in situ* solvothermal method to prepare $LiFePO_4$/graphene followed by a carbon coating process. The composite exhibited a high initial discharge capacity of 163.7 mA h g^{-1} at 0.1 C and 114 mA h g^{-1} at 5 C, as well as an improved cycling stability.

6 Graphene for hybrid energy storage systems

While LIBs offer a higher energy density than SCs, the former suffer from a limited cycle life (100–500 cycles) and low power density. SCs can be charged in minutes or even seconds. Therefore, a combination of the high energy density of LIBs and the high power density and long cycle life of SCs would boost the device performance. This idea has led to the emergence of hybrid energy storage devices or hybrid supercapacitors (HSCs), which indeed exhibit significantly improved electrochemical properties in comparison with LIBs and SCs. HSCs are the integration of a battery-type electrode (such as MnO_2, V_2O_5, $LiCoO_2$, $LiMn_2O_4$, $Li_4Ti_5O_{12}$, *etc.*) with a capacitive electrode as a two electrode device.[269] It should be noted that HSCs based on intercalation compounds containing Li element represent a great promise for applications due to their high capacitance, high power density and excellent cycling behaviour. Amatucci *et al.*[270] first demonstrated the feasibility of HSCs using $Li_4Ti_5O_{12}$ as the negative electrode and AC as the positive electrode and $LiBF_4$ in acetonitrile as the electrolyte (see Fig. 19). The use of $Li_4Ti_5O_{12}$ enabled the device to be operated at 2.25 V. The combination of a high operating voltage and the large specific capacity led to an energy density of 20 W h kg^{-1}. With amorphous MnO_2 as the negative electrode and AC as the positive electrode, about 95% of the initial capacitance was obtained after 23 000 full cycles.[271] In an AC//$LiMn_2O_4$ HSC, the energy density based on the active electrode material was as high as 50 W h kg^{-1} with an excellent power density.[272]

Although intercalated compounds possess a high energy density and wide operating voltage, they normally exhibit low electron and ion conductivities, inhibiting the device performance. Therefore, excellent electrically conductive materials

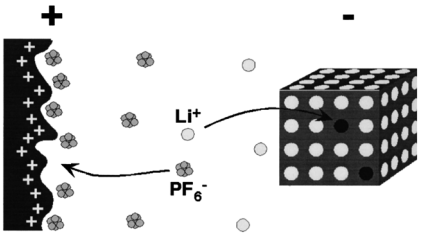

Fig. 19 Schematic of electrode reactions of an asymmetric hybrid cell. Reproduced with permission.[270]

such as carbon nanotubes and graphene have been used to enhance the electrochemical properties of the intercalated compound.[179,202,240,273–279] Zhang *et al.*[280] recently demonstrated an HSC with graphene–RuO_2 as the anode and graphene–PANi as the cathode. The device exhibited an energy density of 26.3 W h kg^{-1}, about two times higher than that of symmetric capacitors of graphene–RuO_2 (12.4 W h kg^{-1}) and graphene–PANi (13.9 W h kg^{-1}) electrodes. Other graphene-containing composite electrodes including MnO_2–graphene,[179,277,281] PANi–graphene,[164,166–168] NiO–graphene,[180–182] $Ni(OH)_2$–graphene,[186] and $Li_4Ti_5O_{12}$–graphene[278,282] have also been studied for hybrid systems.

Chemically activated graphene was used as the cathode and $Li_4Ti_5O_{12}$ as the anode for Li-ion SCs.[283] The results showed that the activated graphene worked well in a full hybrid cell with a specific capacitance as high as 266 F g^{-1} for the active material at an operating potential of 4.0 V with a gravimetric energy density of 53.2 W h kg^{-1} for a packaged cell (based on anode and cathode materials). Very recently, it was demonstrated that pre-lithiated carbon showed improved electrochemical properties as electrodes for Li-ion capacitors.[284–286] Based on these facts, it can be deduced that all-carbon based hybrid SCs and flexible graphene HSCs could be achieved as superior energy storage devices.

7 Graphene for Li–O_2 and Li–S batteries

LIBs and SCs have found applications in niche areas, such as portable electronics. It is envisioned that these devices will play a key role in the electrification of automobile vehicles and stationary electricity storage.[287] However, the energy stored in the currently available devices is too low to meet the demands from the transportation and smart grid industries. Li–O_2 and Li–S batteries with theoretical specific energy densities of 2567 and 3500 W h kg^{-1} respectively are receiving intense interest. The current technology has developed to practical specific energy densities in the range of 300–600 and 500–900 W h kg^{-1} for Li–S and Li–O_2, respectively.[28,288,289] Fig. 20 schematically illustrates the working principle of Li–O_2 and Li–S batteries. Although both types of batteries share the same anode, they are fundamentally different in terms of the electrochemistry of O and S.

7.1 Li–O_2 batteries

The Li–O_2 battery consists of a porous cathode (or oxygen electrode) and a pure lithium anode separated by a lithium-ion conducting electrolyte. The theoretical operating voltage of the Li–O_2 redox couple in an aqueous solution is fairly high, 2.98 V

in the case of alkaline electrolytes and 3.72 V in the case of acidic electrolytes.[289] Because the Li–O_2 battery needs oxygen to complete the electrochemical reaction, a porous material with a good electrical conductivity is generally used as the cathode. 2D graphene has been shown to allow access to oxygen from both sides.[290] Porous graphene (see Fig. 21) was found to deliver an exceptionally high capacity of 15 000 mA h g^{-1} in a Li–O_2 battery.[291] This excellent performance is attributed to the unique bimodal porous structure of the electrode whose microporous channels can facilitate rapid O_2 diffusion and provide high density of reactive sites for Li–O_2 reactions. The surface oxygen-containing groups were observed to react with Li^+ to form isolated nanosized Li_2O_2 particles and help prevent air blocking in the O_2 electrode. Zhou *et al.*[290,292] investigated nitrogen-doped graphene as a metal-free oxygen electrode for reducing oxygen in Li–O_2 batteries. Nitrogen doping can also introduce edge states and defects in graphene, which might serve as active sites for oxygen-reduction.[52,143,293–296] Other elements such as B and S have also been shown to enhance electrochemical activities when doped in graphene.[293,297–300] A reduction in asymmetry between the charge–discharge overpotentials improved the round trip efficiency of Li–O_2 batteries by incorporating a Pt–Au/carbon bifunctional catalyst into a carbon cathode.[301] Some results showed that the catalyst may have triple functions toward increasing the charge capacity, decreasing the charge overpotential and improving cyclability.[302] PtAu alloy was found to enhance the kinetics of oxygen reduction reaction and oxygen evolution reaction.[301,303] This bifunctional catalyst displayed the highest round trip efficiency of Li–O_2 batteries.[303] Composite materials consisting of a metal oxide such as Co_3O_4 or MnO_2 and graphene have been investigated for Li–O_2 batteries.[304–307] Up to now, MnO_2-based and perovskite catalysts are considered as having the most favourable combination of activity and price.[305,307–310]

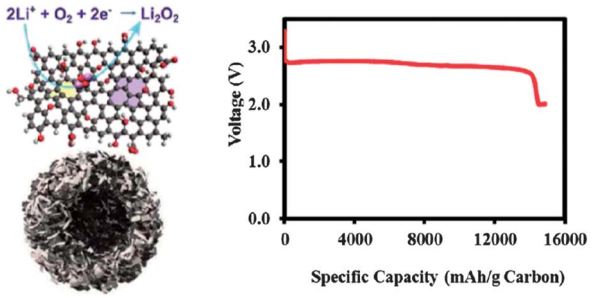

Fig. 21 Scheme illustrating electrochemical reactions on graphene and the discharge curve of a Li–O_2 battery based on a porous graphene electrode. Reproduced with permission.[291]

7.2 Graphene for Li–S batteries

Sulfur is a promising cathode material with a theoretical specific capacity of 1672 mA h g^{-1} (Li_2S), about five times higher than that of traditional cathode materials based on transition metal oxides or phosphates.[311] However, several problems hinder its applications, such as poor rechargability and limited rate capability owing to the insulating nature of sulfur and the formation of solid reduction products (Li_2S and Li_2S_2), fast capacity fading owing to the formation of soluble polysulfide intermediates (leading to a shuttle mechanism), and poorly controlled Li/electrolyte interface.[312] Various carbon–sulfur and conducting polymer–sulfur composites have been described with the specific capacity exceeding 1000 mA h g^{-1}.[288,313–315] However, it remains challenging to retain high and stable capacity of a sulfur cathode with a long cycle life.

Mixing graphene with sulfur followed by heat treatments at a temperature higher than the melting point of sulfur to form graphene-coated sulphur was demonstrated.[316] Although the composite showed an improved capacity and cycle life in comparison with a bare sulfur electrode, the problem of forming a soluble polysulfide intermediate was not solved. Graphene-wrapped sulfur particles and polymer-coated sulfur–graphene composites have been shown to display an enhanced electric conductivity and address polysulfide solubility.[317–319] Cui *et al.*[317] demonstrated that graphene wrapped sulfur composites showed high and stable specific capacities of up to ~600 mA h g^{-1} over more than 100 cycles with a high energy density (Fig. 22). The poly(ethylene glycol) (PEG) and graphene

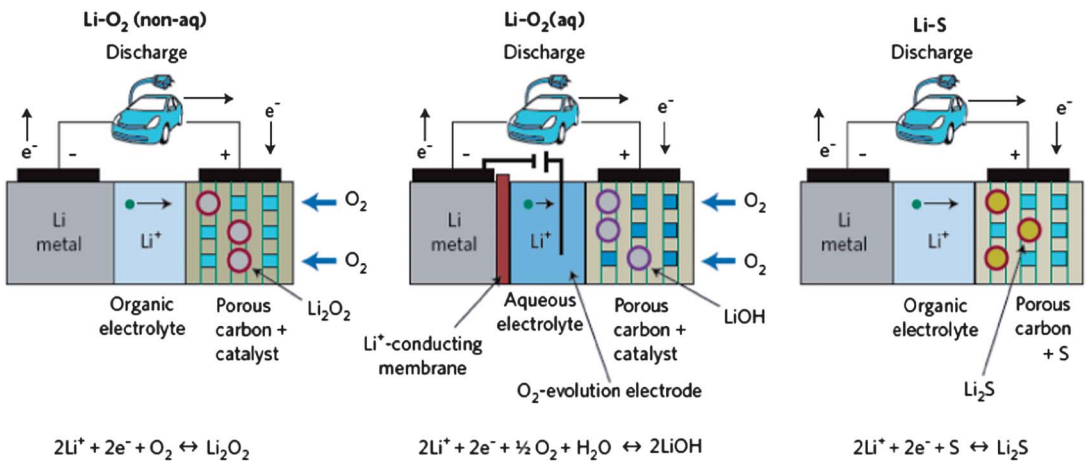

Fig. 20 Schematic diagrams of non-aqueous and aqueous Li–O_2 and Li–S cells. Reproduced with permission.[28]

coating layers are important to accommodate volume expansion, to trap the soluble polysulfide intermediate, and to render the sulfur particles electrically conducting. However, PEG is an electrically insulating material, which may lower the overall electrochemical performance of the composite material. However, if a conducting polymer such as polypyrrole and polyaniline carbon is introduced to graphene–sulfur composites, the ternary composite exhibited superior lithium storage properties as demonstrated by Nazar *et al.*[320] Zhang *et al.*[321] coated a uniform and thin layer of sulfur coating on GO. The composite displayed a high reversible capacity of 950–1400 mA h g^{-1} and stable cycling for more than 50 cycles at 0.1 C because of the strong interaction between GO and sulfur or polysulfides. However, as GO has a poor electric conductivity, it is not suitable for high-rate batteries. Considering the simple synthesis and low cost of the composites, further incorporating this approach with conducting polymers or mesoporous carbon electrodes may offer a very interesting way forward.

While both batteries have been investigated intensively, they are still far from practical applications. It is important that future work focuses on understanding the fundamental chemistry of the Li–O_2 and Li–S batteries if advances have been made.

8 Summary and perspectives

The application of graphene as an electrode for energy storage devices is a rapidly advancing field. While considerable research progress and breakthroughs have been achieved in this field over the past few years, challenges of using graphene for energy storage remain. Several problems must be solved before this lightest and most electrically conductive material known is practically used in electrochemical energy storage devices.

Firstly, a cost-effective and environmentally friendly approach to large-scale production of graphene or reduced graphene oxide or graphene nanoplatelets must be available. As graphite is abundant in nature and readily available, beginning from graphite to produce graphene or its derivatives is still the most ideal route. While the physical exfoliation method discovered by Geim and co-workers[17] allows one to obtain pristine single layer graphene, it is not suitable for mass production. In addition, the exfoliated single-layer graphene sheets tend to restack to form thick platelets. On the other hand, the chemical method that leads to the formation of graphene oxide or intercalated graphite must be followed by subsequent processing steps, such as thermal or mechanical decomposition, ball milling, and reduction, which create additional cost and environmental problems.

As a result, advanced material processing methods to convert graphite to graphene or its derivative with desired properties will continue to gain substantial research interests in the coming years.

Second, while graphene has a high theoretical specific surface area, the surface of graphene is hardly completely available due to restacking or aggregation of the primary sheets during materials processing and device fabrication processes. 3D porous architectures with graphene sheets as the primary building blocks are the most desirable electrode materials in energy storage. Pillaring graphene sheets with carbon nanotubes as has been demonstrated previously[161,162] represents a promising approach to fabricating such architectures.

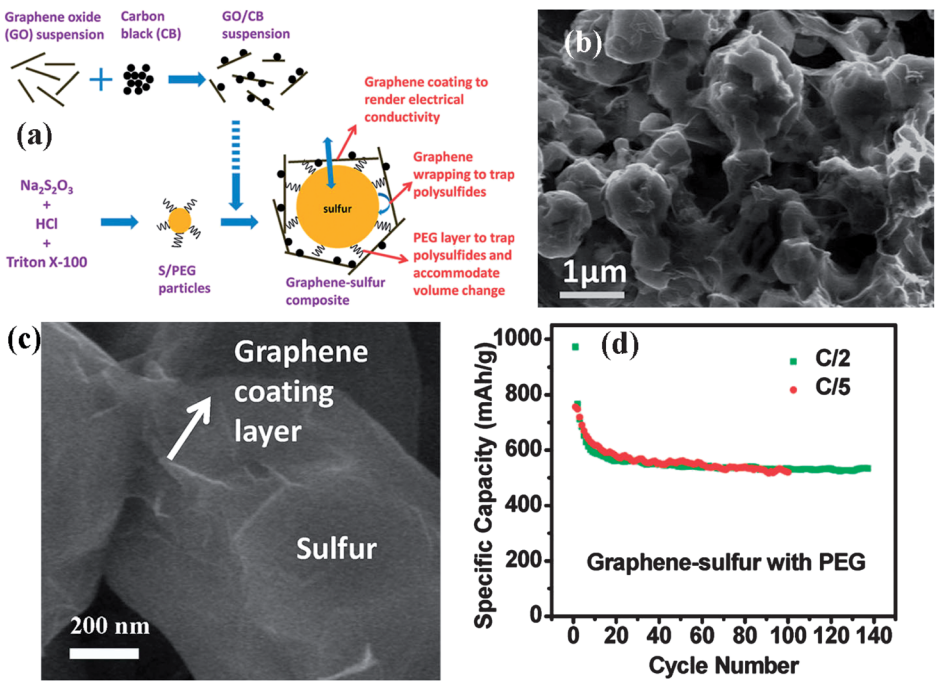

Fig. 22 (a) Schematic illustration of the preparation of a graphene–sulfur composite; (b and c) SEM images of the graphene–sulfur composite; (d) cycling performance of the composite at rates of 0.2 and 0.5 C, respectively. Reproduced with permission.[317]

Third, graphene-based composite materials with the advantageous properties of both graphene and the guest component show significantly improved performance in many energy storage configurations, especially in asymmetric supercapacitors. It is very likely that graphene-based composites will soon find applications in the supercapacitor industry to replace (or partially replace) activated carbon. With the rapid advancement in the development of cathode materials for Li-ion batteries, Si–graphene composite electrodes may kick graphite out of the market in the battery industry. All in all, finding a simple and cost-effective method to make graphene-based composite materials with a high stability against various harsh environments encountered during electrode fabrication, charging and discharging processes, and in acidic or caustic electrolyte is challenging.

Fourth, flexible, light and all-solid-state energy storage devices with high energy and power densities will continue to gain increased research attention. Asymmetric supercapacitors and hybrid energy storage systems with 3D porous graphene-based architectures as the electrode and safe and non-harmful ionic liquids as the electrolyte are believed to be the future research focus.

Fifth, Li–O_2 and Li–S batteries may lead a revolution in the energy storage history. Both batteries represent advantages in minimizing the cost of cells compared with lithium-ion batteries. The key problems associated with Li–O_2 and Li–S batteries[311] have not been completely solved until now. It is important that future work focuses on understanding the fundamental chemistry in these two cells if progress is to be made.

Last but not least, experimental and theoretical fundamental studies on ion transport behaviour at the surface and cross-electrode films under device working conditions can be of great help in both electrode design and device configuration.

Acknowledgements

This work was financially supported by the Australian Research Council (ARC) Future Fellow Program of project number FT100100879.

Notes and references

1 A. K. Geim and K. S. Novoselov, *Nat. Mater.*, 2007, **6**, 183–191.
2 I. Calizo, A. A. Balandin, W. Bao, F. Miao and C. N. Lau, *Nano Lett.*, 2007, **7**, 2645–2649.
3 A. A. Balandin, *Nat. Mater.*, 2011, **10**, 569–581.
4 D. L. Nika and A. A. Balandin, *J. Phys.: Condens. Matter*, 2012, **24**, 233203.
5 S. De and J. N. Coleman, *ACS Nano*, 2010, **4**, 2713–2720.
6 J. C. Meyer, A. K. Geim, M. I. Katsnelson, K. S. Novoselov, T. J. Booth and S. Roth, *Nature*, 2007, **446**, 60–63.
7 C. R. Dean, A. F. Young, I. Meric, C. Lee, L. Wang, S. Sorgenfrei, K. Watanabe, T. Taniguchi, P. Kim, K. L. Shepard and J. Hone, *Nat. Nanotechnol.*, 2010, **5**, 722–726.
8 Y. H. Lu, M. Zhou, C. Zhang and Y. P. Feng, *J. Phys. Chem. C*, 2009, **113**, 20156–20160.
9 T. Xue, S. Jiang, Y. Qu, Q. Su, R. Cheng, S. Dubin, C.-Y. Chiu, R. Kaner, Y. Huang and X. Duan, *Angew. Chem., Int. Ed.*, 2012, **51**, 3822–3825.
10 S. Stankovich, D. A. Dikin, G. H. B. Dommett, K. M. Kohlhaas, E. J. Zimney, E. A. Stach, R. D. Piner, S. T. Nguyen and R. S. Ruoff, *Nature*, 2006, **442**, 282–286.
11 T. Ramanathan, A. A. Abdala, S. Stankovich, D. A. Dikin, M. Herrera-Alonso, R. D. Piner, D. H. Adamson, H. C. Schniepp, X. Chen, R. S. Ruoff, S. T. Nguyen, I. A. Aksay, R. K. Prud'homme and L. C. Brinson, *Nat. Nanotechnol.*, 2008, **3**, 327–331.
12 M. F. El-Kady, V. Strong, S. Dubin and R. B. Kaner, *Science*, 2012, **335**, 1326–1330.
13 J. T. Zhang, Z. G. Xiong and X. S. Zhao, *J. Mater. Chem.*, 2011, **21**, 3634–3640.
14 Z. G. Xiong, L. L. Zhang and X. S. Zhao, *Chem.–Eur. J.*, 2011, **17**, 2428–2434.
15 Z. G. Xiong, L. L. Zhang, J. Z. Ma and X. S. Zhao, *Chem. Commun.*, 2010, **46**, 6099–6101.
16 J. Z. Ma, J. T. Zhang, Z. G. Xiong, Y. Yong and X. S. Zhao, *J. Mater. Chem.*, 2011, **21**, 3350–3352.
17 K. S. Novoselov, A. K. Geim, S. V. Morozov, D. Jiang, Y. Zhang, S. V. Dubonos, I. V. Grigorieva and A. A. Firsov, *Science*, 2004, **306**, 666–669.
18 D. A. Dikin, S. Stankovich, E. J. Zimney, R. D. Piner, G. H. B. Dommett, G. Evmenenko, S. T. Nguyen and R. S. Ruoff, *Nature*, 2007, **448**, 457–460.
19 S. Park and R. S. Ruoff, *Nat. Nanotechnol.*, 2009, **4**, 217–224.
20 D. Li, M. B. Muller, S. Gilje, R. B. Kaner and G. G. Wallace, *Nat. Nanotechnol.*, 2008, **3**, 101–105.
21 D. R. Dreyer, S. Park, C. W. Bielawski and R. S. Ruoff, *Chem. Soc. Rev.*, 2010, **39**, 228–240.
22 A. S. Arico, P. Bruce, B. Scrosati, J. M. Tarascon and W. Van Schalkwijk, *Nat. Mater.*, 2005, **4**, 366–377.
23 Y. Gogotsi and P. Simon, *Science*, 2011, **334**, 917–918.
24 B. Dunn, H. Kamath and J.-M. Tarascon, *Science*, 2011, **334**, 928–935.
25 J. B. Goodenough and Y. Kim, *Chem. Mater.*, 2010, **22**, 587–603.
26 P. Simon and Y. Gogotsi, *Nat. Mater.*, 2008, **7**, 845–854.
27 L. L. Zhang, R. Zhou and X. S. Zhao, *J. Mater. Chem.*, 2010, **20**, 5983–5992.
28 P. G. Bruce, S. A. Freunberger, L. J. Hardwick and J. M. Tarascon, *Nat. Mater.*, 2012, **11**, 19–29.
29 M. Terrones, A. R. Botello-Mendez, J. Campos-Delgado, F. Lopez-Urias, Y. I. Vega-Cantu, F. J. Rodriguez-Macias, A. L. Elias, E. Munoz-Sandoval, A. G. Cano-Marquez, J. C. Charlier and H. Terrones, *Nano Today*, 2010, **5**, 351–372.
30 M. J. Allen, V. C. Tung and R. B. Kaner, *Chem. Rev.*, 2010, **110**, 132–145.
31 Y. W. Zhu, S. Murali, W. W. Cai, X. S. Li, J. W. Suk, J. R. Potts and R. S. Ruoff, *Adv. Mater.*, 2010, **22**, 3906–3924.
32 D. Chen, L. H. Tang and J. H. Li, *Chem. Soc. Rev.*, 2010, **39**, 3157–3180.

33 K. S. Novoselov, A. K. Geim, S. V. Morozov, D. Jiang, M. I. Katsnelson, I. V. Grigorieva, S. V. Dubonos and A. A. Firsov, *Nature*, 2005, **438**, 197–200.
34 Y. Zhang, Y.-W. Tan, H. L. Stormer and P. Kim, *Nature*, 2005, **438**, 201–204.
35 M. Pumera, *Energy Environ. Sci.*, 2011, **4**, 668–674.
36 C. Gomez-Navarro, R. T. Weitz, A. M. Bittner, M. Scolari, A. Mews, M. Burghard and K. Kern, *Nano Lett.*, 2007, **7**, 3499–3503.
37 Z. Chen, H. Yuan, Y. Zhang, K. Nomura, T. Gao, Y. Gao, H. Shimotani, Z. Liu and Y. Iwasa, *Nano Lett.*, 2012, **7**, 238–242.
38 D. Graf, F. Molitor, K. Ensslin, C. Stampfer, A. Jungen, C. Hierold and L. Wirtz, *Nano Lett.*, 2007, **7**, 238–242.
39 J. E. Proctor, E. Gregoryanz, K. S. Novoselov, M. Lotya, J. N. Coleman and M. P. Halsall, *Phys. Rev. B: Condens. Matter Mater. Phys.*, 2009, **80**, 073408.
40 Y. F. Hao, Y. Y. Wang, L. Wang, Z. H. Ni, Z. Q. Wang, R. Wang, C. K. Koo, Z. X. Shen and J. T. L. Thong, *Small*, 2010, **6**, 195–200.
41 S. G. S. V. P. Gusynin and J. P. Carbotte, *Phys. Rev. Lett.*, 2006, **96**, 256802.
42 S. Bae, H. Kim, Y. Lee, X. Xu, J.-S. Park, Y. Zheng, J. Balakrishnan, T. Lei, H. Ri Kim, Y. I. Song, Y.-J. Kim, K. S. Kim, B. Ozyilmaz, J.-H. Ahn, B. H. Hong and S. Iijima, *Nat. Nanotechnol.*, 2010, **5**, 574–578.
43 V. Goyal and A. A. Balandin, *Appl. Phys. Lett.*, 2012, **100**, 073113.
44 K. M. F. Shahil and A. A. Balandin, *Nano Lett.*, 2012, **12**, 861–867.
45 C. Gomez-Navarro, M. Burghard and K. Kern, *Nano Lett.*, 2008, **8**, 2045–2049.
46 C. Lee, X. D. Wei, J. W. Kysar and J. Hone, *Science*, 2008, **321**, 385–388.
47 A. R. Ranjbartoreh, B. Wang, X. P. Shen and G. X. Wang, *J. Appl. Phys.*, 2011, **109**, 014306.
48 K. S. Kim, Y. Zhao, H. Jang, S. Y. Lee, J. M. Kim, J. H. Ahn, P. Kim, J. Y. Choi and B. H. Hong, *Nature*, 2009, **457**, 706–710.
49 L. S. Panchokarla, K. S. Subrahmanyam, S. K. Saha, A. Govindaraj, H. R. Krishnamurthy, U. V. Waghmare and C. N. R. Rao, *Adv. Mater.*, 2009, **21**, 4726–4730.
50 N. Al-Aqtash and I. Vasiliev, *J. Phys. Chem. C*, 2011, **115**, 18500–18510.
51 Y. Li, Y. Zhao, H. Cheng, Y. Hu, G. Shi, L. Dai and L. Qu, *J. Am. Chem. Soc.*, 2011, **134**, 15–18.
52 X. R. Wang, X. L. Li, L. Zhang, Y. Yoon, P. K. Weber, H. L. Wang, J. Guo and H. J. Dai, *Science*, 2009, **324**, 768–771.
53 O. C. Compton, D. A. Dikin, K. W. Putz, L. C. Brinson and S. T. Nguyen, *Adv. Mater.*, 2010, **22**, 892–896.
54 L. T. Qu, Y. Liu, J. B. Baek and L. M. Dai, *ACS Nano*, 2010, **4**, 1321–1326.
55 S. J. Guo and S. J. Dong, *Chem. Soc. Rev.*, 2011, **40**, 2644–2672.
56 Y. Q. Liu, L. Gao, S. Zheng, Y. Wang, J. Sun, H. Kajiura, Y. Li and K. Noda, *Nanotechnology*, 2007, **18**, 365702.
57 A. B. Artyukhin, O. Bakajin, P. Stroeve and A. Noy, *Langmuir*, 2004, **20**, 1442–1448.
58 P. G. He and M. Bayachou, *Langmuir*, 2005, **21**, 6086–6092.
59 H. Paloniemi, M. Lukkarinen, T. Aaritalo, S. Areva, J. Leiro, M. Heinonen, K. Haapakka and J. Lukkari, *Langmuir*, 2006, **22**, 74–83.
60 J. H. Rouse and P. T. Lillehei, *Nano Lett.*, 2003, **3**, 59–62.
61 A. A. Mamedov, N. A. Kotov, M. Prato, D. M. Guldi, J. P. Wicksted and A. Hirsch, *Nat. Mater.*, 2002, **1**, 190–194.
62 J. L. Sabourin, D. M. Dabbs, R. A. Yetter, F. L. Dryer and I. A. Aksay, *ACS Nano*, 2009, **3**, 3945–3954.
63 Y. Chen, X. Zhang, P. Yu and Y. W. Ma, *Chem. Commun.*, 2009, 4527–4529.
64 Z. H. Tang, C. F. Zeng, Y. D. Lei, B. C. Guo, L. Q. Zhang and D. M. Jia, *J. Mater. Chem.*, 2011, **21**, 17111–17118.
65 S. C. Lin, C. J. Shih, M. S. Strano and D. Blankschtein, *J. Am. Chem. Soc.*, 2011, **133**, 12810–12823.
66 J. Q. Tian, H. L. Li, Y. L. Luo, L. Wang, Y. W. Zhang and X. P. Sun, *Langmuir*, 2011, **27**, 874–877.
67 A. Rani, K. A. Oh, H. Koo, H. J. Lee and M. Park, *Appl. Surf. Sci.*, 2011, **257**, 4982–4989.
68 P. Hasin, M. A. Alpuche-Aviles and Y. Y. Wu, *J. Phys. Chem. C*, 2010, **114**, 15857–15861.
69 Y. X. Fang, S. J. Guo, C. Z. Zhu, Y. M. Zhai and E. K. Wang, *Langmuir*, 2010, **26**, 11277–11282.
70 D. G. Wang and X. G. Wang, *Langmuir*, 2011, **27**, 2007–2013.
71 X. Y. Qi, K. Y. Pu, X. Z. Zhou, H. Li, B. Liu, F. Boey, W. Huang and H. Zhang, *Small*, 2010, **6**, 663–669.
72 X. B. Fan, W. C. Peng, Y. Li, X. Y. Li, S. L. Wang, G. L. Zhang and F. B. Zhang, *Adv. Mater.*, 2008, **20**, 4490–4493.
73 J. Gao, F. Liu, Y. L. Liu, N. Ma, Z. Q. Wang and X. Zhang, *Chem. Mater.*, 2010, **22**, 2213–2218.
74 M. J. Fernandez-Merino, L. Guardia, J. I. Paredes, S. Villar-Rodil, P. Solis-Fernandez, A. Martinez-Alonso and J. M. D. Tascon, *J. Phys. Chem. C*, 2010, **114**, 6426–6432.
75 C. Z. Zhu, S. J. Guo, Y. X. Fang and S. J. Dong, *ACS Nano*, 2010, **4**, 2429–2437.
76 Y. Zhou, Q. L. Bao, L. A. L. Tang, Y. L. Zhong and K. P. Loh, *Chem. Mater.*, 2009, **21**, 2950–2956.
77 S. Dubin, S. Gilje, K. Wang, V. C. Tung, K. Cha, A. S. Hall, J. Farrar, R. Varshneya, Y. Yang and R. B. Kaner, *ACS Nano*, 2010, **4**, 3845–3852.
78 G. X. Wang, B. Wang, J. Park, J. Yang, X. P. Shen and J. Yao, *Carbon*, 2009, **47**, 68–72.
79 H. P. Viet, V. C. Tran, S. H. Hur, E. Oh, E. J. Kim, E. W. Shin and J. S. Chung, *J. Mater. Chem.*, 2011, **21**, 3371–3377.
80 H. L. Wang, J. T. Robinson, X. L. Li and H. J. Dai, *J. Am. Chem. Soc.*, 2009, **131**, 9910–9911.
81 H. F. Yang, F. H. Li, C. S. Shan, D. X. Han, Q. X. Zhang, L. Niu and A. Ivaska, *J. Mater. Chem.*, 2009, **19**, 4632–4638.
82 G. P. Keeley, A. O'Neill, M. Holzinger, S. Cosnier, J. N. Coleman and G. S. Duesberg, *Phys. Chem. Chem. Phys.*, 2011, **13**, 7747–7750.
83 Z. J. F. Z. J. Fan, W. Kai, J. Yan, T. Wei, L. J. Zhi, J. Feng, Y. M. Ren, L. P. Song and F. Wei, *ACS Nano*, 2011, **5**, 191–198.
84 X. G. Mei and J. Y. Ouyang, *Carbon*, 2011, **49**, 5389–5397.

85 G. Williams, B. Seger and P. V. Kamat, *ACS Nano*, 2008, **2**, 1487–1491.
86 P. V. Kamat, *J. Phys. Chem. Lett.*, 2010, **1**, 520–527.
87 Z. G. Xiong, J. Z. Ma, W. J. Ng, T. D. Waite and X. S. Zhao, *Water Res.*, 2011, **45**, 2095–2103.
88 Z. G. Xiong, H. Q. Dou, J. H. Pan, J. Z. Ma, C. Xu and X. S. Zhao, *CrystEngComm*, 2010, **12**, 3455–3457.
89 Z. G. Xiong and X. S. Zhao, *J. Am. Chem. Soc.*, 2012, **134**, 5754–5757.
90 J. Z. Ma, Z. G. Xiong, T. D. Waite, W. J. Ng and X. S. Zhao, *Microporous Mesoporous Mater.*, 2011, **144**, 97–104.
91 X. Q. An and J. C. Yu, *RSC Adv.*, 2011, **1**, 1426–1434.
92 G. Williams and P. V. Kamat, *Langmuir*, 2009, **25**, 13869–13873.
93 H. Li, S. Pang, X. Feng, K. Mullen and C. Bubeck, *Chem. Commun.*, 2010, **46**, 6243–6245.
94 H. L. Li, S. P. Pang, S. Wu, X. L. Feng, K. Mullen and C. Bubeck, *J. Am. Chem. Soc.*, 2011, **133**, 9423–9429.
95 Y. H. Ng, A. Iwase, N. J. Bell, A. Kudo and R. Amal, *Catal. Today*, 2011, **164**, 353–357.
96 Q. Li, B. D. Guo, J. G. Yu, J. R. Ran, B. H. Zhang, H. J. Yan and J. R. Gong, *J. Am. Chem. Soc.*, 2011, **133**, 10878–10884.
97 A. Iwase, Y. H. Ng, Y. Ishiguro, A. Kudo and R. Amal, *J. Am. Chem. Soc.*, 2011, **133**, 11054–11057.
98 A. Mukherji, B. Seger, G. Q. Lu and L. Wang, *ACS Nano*, 2011, **5**, 3483–3492.
99 J.-W. Jang, S. Cho, G.-h. Moon, K. Ihm, J. Y. Kim, D. H. Youn, S. Lee, Y. h. Lee, W. Choi, K.-H. Lee and J. S. Lee, *Chem.–Eur. J.*, 2012, **18**, 2762–2767.
100 X. S. Li, W. W. Cai, J. H. An, S. Kim, J. Nah, D. X. Yang, R. Piner, A. Velamakanni, I. Jung, E. Tutuc, S. K. Banerjee, L. Colombo and R. S. Ruoff, *Science*, 2009, **324**, 1312–1314.
101 X. S. Li, W. W. Cai, L. Colombo and R. S. Ruoff, *Nano Lett.*, 2009, **9**, 4268–4272.
102 A. Reina, X. Jia, J. Ho, D. Nezich, H. Son, V. Bulovic, M. S. Dresselhaus and J. Kong, *Nano Lett.*, 2008, **9**, 30–35.
103 K. S. Kim, Y. Zhao, H. Jang, S. Y. Lee, J. M. Kim, K. S. Kim, J.-H. Ahn, P. Kim, J.-Y. Choi and B. H. Hong, *Nature*, 2009, **457**, 706–710.
104 Z. P. Chen, W. C. Ren, L. B. Gao, B. L. Liu, S. F. Pei and H. M. Cheng, *Nat. Mater.*, 2011, **10**, 424–428.
105 F. Xiao, J. B. Song, H. C. Gao, X. L. Zan, R. Xu and H. W. Duan, *ACS Nano*, 2012, **6**, 100–110.
106 H. Bi, F. Q. Huang, J. Liang, Y. F. Tang, X. J. Lu, X. M. Xie and M. H. Jiang, *J. Mater. Chem.*, 2011, **21**, 17366–17370.
107 F. Yavari, Z. P. Chen, A. V. Thomas, W. C. Ren, H. M. Cheng and N. Koratkar, *Sci. Rep.*, 2011, **1**, 166.
108 X. H. Cao, Y. M. Shi, W. H. Shi, G. Lu, X. Huang, Q. Y. Yan, Q. C. Zhang and H. Zhang, *Small*, 2011, **7**, 3163–3168.
109 L. B. Gao, W. C. Ren, J. P. Zhao, L. P. Ma, Z. P. Chen and H. M. Cheng, *Appl. Phys. Lett.*, 2010, **97**, 183109.
110 S. Bhaviripudi, X. T. Jia, M. S. Dresselhaus and J. Kong, *Nano Lett.*, 2010, **10**, 4128–4133.
111 H. X. Ji, Y. F. Hao, Y. J. Ren, M. Charlton, W. H. Lee, Q. Z. Wu, H. F. Li, Y. W. Zhu, Y. P. Wu, R. Piner and R. S. Ruoff, *ACS Nano*, 2011, **5**, 7656–7661.
112 Z. C. Li, P. Wu, C. X. Wang, X. D. Fan, W. H. Zhang, X. F. Zhai, C. G. Zeng, Z. Y. Li, J. L. Yang and J. G. Hou, *ACS Nano*, 2011, **5**, 3385–3390.
113 G. D. Ruan, Z. Z. Sun, Z. W. Peng and J. M. Tour, *ACS Nano*, 2011, **5**, 7601–7607.
114 Z. Z. Sun, Z. Yan, J. Yao, E. Beitler, Y. Zhu and J. M. Tour, *Nature*, 2010, **468**, 549–552.
115 J. Hofrichter, B. N. Szafranek, M. Otto, T. J. Echtermeyer, M. Baus, A. Majerus, V. Geringer, M. Ramsteiner and H. Kurz, *Nano Lett.*, 2010, **10**, 36–42.
116 H. Park, P. R. Brown, V. Buloyic and J. Kong, *Nano Lett.*, 2012, **12**, 133–140.
117 Y. Wang, Y. Zheng, X. Xu, E. Dubuisson, Q. Bao, J. Lu and K. P. Loh, *ACS Nano*, 2011, **5**, 9927–9933.
118 L. Gao, W. Ren, H. Xu, L. Jin, Z. Wang, T. Ma, L.-P. Ma, Z. Zhang, Q. Fu, L.-M. Peng, X. Bao and H.-M. Cheng, *Nat. Commun.*, 2012, **3**, 699.
119 H. J. Dai, *Acc. Chem. Res.*, 2002, **35**, 1035–1044.
120 Z. S. Wu, W. C. Ren, L. B. Gao, J. P. Zhao, Z. P. Chen, B. L. Liu, D. M. Tang, B. Yu, C. B. Jiang and H. M. Cheng, *ACS Nano*, 2009, **3**, 411–417.
121 K. S. Subrahmanyam, L. S. Panchakarla, A. Govindaraj and C. N. R. Rao, *J. Phys. Chem. C*, 2009, **113**, 4257–4259.
122 Z. Y. Wang, N. Li, Z. J. Shi and Z. N. Gu, *Nanotechnology*, 2010, **21**, 175602.
123 B. N. Wanjala, J. Luo, R. Loukrakpam, B. Fang, D. Mott, P. N. Njoki, M. Engelhard, H. R. Naslund, J. K. Wu, L. C. Wang, O. Malis and C. J. Zhong, *Chem. Mater.*, 2010, **22**, 4282–4294.
124 C. G. Salzmann, V. Nicolosi and M. L. H. Green, *J. Mater. Chem.*, 2010, **20**, 314–319.
125 Z. X. Chen, M. Zhou, Y. L. Cao, X. P. Ai, H. X. Yang and J. Liu, *Adv. Energy Mater.*, 2012, **2**, 95–102.
126 Y. C. Fan, L. J. Wang, J. L. Li, J. Q. Li, S. K. Sun, F. Chen, L. D. Chen and W. Jiang, *Carbon*, 2010, **48**, 1743–1749.
127 V. Leon, M. Quintana, M. A. Herrero, J. L. G. Fierro, A. d. l. Hoz, M. Prato and E. Vazquez, *Chem. Commun.*, 2011, **47**, 10936–10938.
128 L. H. Li, Y. Chen, G. Behan, H. Z. Zhang, M. Petravic and A. M. Glushenkov, *J. Mater. Chem.*, 2011, **21**, 11862–11866.
129 I.-Y. Jeon, Y.-R. Shin, G.-J. Sohn, H.-J. Choi, S.-Y. Bae, J. Mahmood, S.-M. Jung, J.-M. Seo, M.-J. Kim, D. Wook Chang, L. Dai and J.-B. Baek, *Proc. Natl. Acad. Sci. U. S. A.*, 2012, **109**, 5588–5593.
130 J. N. Coleman, *Acc. Chem. Res.*, 2013, **46**, 14–22.
131 G. Cunningham, M. Lotya, C. S. Cucinotta, S. Sanvito, S. D. Bergin, R. Menzel, M. S. P. Shaffer and J. N. Coleman, *ACS Nano*, 2012, **6**, 3468–3480.
132 R. J. Smith, P. J. King, M. Lotya, C. Wirtz, U. Khan, S. De, A. O'Neill, G. S. Duesberg, J. C. Grunlan, G. Moriarty, J. Chen, J. Z. Wang, A. I. Minett, V. Nicolosi and J. N. Coleman, *Adv. Mater.*, 2011, **23**, 3944–3948.
133 J. N. Coleman, M. Lotya, A. O'Neill, S. D. Bergin, P. J. King, U. Khan, K. Young, A. Gaucher, S. De, R. J. Smith, I. V. Shvets, S. K. Arora, G. Stanton, H. Y. Kim, K. Lee, G. T. Kim, G. S. Duesberg, T. Hallam, J. J. Boland, J. J. Wang, J. F. Donegan, J. C. Grunlan, G. Moriarty,

A. Shmeliov, R. J. Nicholls, J. M. Perkins, E. M. Grieveson, K. Theuwissen, D. W. McComb, P. D. Nellist and V. Nicolosi, *Science*, 2011, **331**, 568–571.
134 M. Lotya, Y. Hernandez, P. J. King, R. J. Smith, V. Nicolosi, L. S. Karlsson, F. M. Blighe, S. De, Z. Wang, I. T. McGovern, G. S. Duesberg and J. N. Coleman, *J. Am. Chem. Soc.*, 2009, **131**, 3611–3620.
135 C. Y. Su, A. Y. Lu, Y. P. Xu, F. R. Chen, A. N. Khlobystov and L. J. Li, *ACS Nano*, 2011, **5**, 2332–2339.
136 D. Wei, L. Grande, V. Chundi, R. White, C. Bower, P. Andrew and T. Ryhanen, *Chem. Commun.*, 2012, **48**, 1239–1241.
137 J. Z. Wang, K. K. Manga, Q. L. Bao and K. P. Loh, *J. Am. Chem. Soc.*, 2011, **133**, 8888–8891.
138 L. Dossel, L. Gherghel, X. L. Feng and K. Mullen, *Angew. Chem., Int. Ed.*, 2011, **50**, 2540–2543.
139 J. M. Englert, A. Hirsch, X. L. Feng and K. Mullen, *Angew. Chem., Int. Ed.*, 2011, **50**, A17–A24.
140 J. M. Cai, P. Ruffieux, R. Jaafar, M. Bieri, T. Braun, S. Blankenburg, M. Muoth, A. P. Seitsonen, M. Saleh, X. L. Feng, K. Mullen and R. Fasel, *Nature*, 2010, **466**, 470–473.
141 S. Osella, A. Narita, M. G. Schwab, Y. Hernandez, X. L. Feng, K. Mullen and D. Beljonne, *ACS Nano*, 2012, **6**, 5539–5548.
142 P. Avouris, *Nano Lett.*, 2010, **10**, 4285–4294.
143 Y. F. Li, Z. Zhou, P. W. Shen and Z. F. Chen, *ACS Nano*, 2009, **3**, 1952–1958.
144 M. Choucair, P. Thordarson and J. A. Stride, *Nat. Nanotechnol.*, 2009, **4**, 30–33.
145 B. E. Conway, *Electrochemical Supercapacitors: Scientific Fundamentals and Technological Applications*, Kluwer Academic/Plenum Publisher, New York, 1999.
146 H. L. Li, J. X. Wang, Q. X. Chu, Z. Wang, F. B. Zhang and S. C. Wang, *J. Power Sources*, 2009, **190**, 578–586.
147 F. Lufrano, P. Staiti and M. Minutoli, *J. Power Sources*, 2003, **124**, 314–320.
148 L. L. Zhang and X. S. Zhao, *Chem. Soc. Rev.*, 2009, **38**, 2520–2531.
149 M. D. Stoller and R. S. Ruoff, *Energy Environ. Sci.*, 2010, **3**, 1294–1301.
150 Y. P. Zhai, Y. Q. Dou, D. Y. Zhao, P. F. Fulvio, R. T. Mayes and S. Dai, *Adv. Mater.*, 2011, **23**, 4828–4850.
151 M. D. Stoller, S. J. Park, Y. W. Zhu, J. H. An and R. S. Ruoff, *Nano Lett.*, 2008, **8**, 3498–3502.
152 Z. Lei, L. Lu and X. S. Zhao, *Energy Environ. Sci.*, 2012, **5**, 6391–6399.
153 Y. W. Zhu, S. Murali, M. D. Stoller, K. J. Ganesh, W. W. Cai, P. J. Ferreira, A. Pirkle, R. M. Wallace, K. A. Cychosz, M. Thommes, D. Su, E. A. Stach and R. S. Ruoff, *Science*, 2011, **332**, 1537–1541.
154 L. L. Zhang, X. Zhao, M. D. Stoller, Y. Zhu, H. Ji, S. Murali, Y. Wu, S. Perales, B. Clevenger and R. S. Ruoff, *Nano Lett.*, 2012, **12**, 1806–1812.
155 Y. X. Xu, K. X. Sheng, C. Li and G. Q. Shi, *ACS Nano*, 2010, **4**, 4324–4330.
156 G. K. Wang, X. Sun, F. Y. Lu, H. T. Sun, M. P. Yu, W. L. Jiang, C. S. Liu and J. Lian, *Small*, 2012, **8**, 452–459.
157 Z. Lei, N. Christov and X. S. Zhao, *Energy Environ. Sci.*, 2011, **4**, 1866–1873.
158 U. Khan, I. O'Connor, Y. K. Gun'ko and J. N. Coleman, *Carbon*, 2010, **48**, 2825–2830.
159 K. S. Kim and S. J. Park, *Electrochim. Acta*, 2011, **56**, 1629–1635.
160 Z. Sui, Q. Meng, X. Zhang, R. Ma and B. Cao, *J. Mater. Chem.*, 2012, **22**, 8767–8771.
161 L. L. Zhang, Z. G. Xiong and X. S. Zhao, *ACS Nano*, 2010, **4**, 7030–7036.
162 Z. J. Fan, J. Yan, L. J. Zhi, Q. Zhang, T. Wei, J. Feng, M. L. Zhang, W. Z. Qian and F. Wei, *Adv. Mater.*, 2010, **22**, 3723–3728.
163 A. V. Murugan, T. Muraliganth and A. Manthiram, *Chem. Mater.*, 2009, **21**, 5004–5006.
164 K. Zhang, L. L. Zhang, X. S. Zhao and J. S. Wu, *Chem. Mater.*, 2010, **22**, 1392–1401.
165 C. H. Xu, J. Sun and L. Gao, *J. Mater. Chem.*, 2011, 11253–11258.
166 J. J. Xu, K. Wang, S. Z. Zu, B. H. Han and Z. X. Wei, *ACS Nano*, 2010, **4**, 5019–5026.
167 Q. Wu, Y. X. Xu, Z. Y. Yao, A. R. Liu and G. Q. Shi, *ACS Nano*, 2010, **4**, 1963–1970.
168 D. W. Wang, F. Li, J. P. Zhao, W. C. Ren, Z. G. Chen, J. Tan, Z. S. Wu, I. Gentle, G. Q. Lu and H. M. Cheng, *ACS Nano*, 2009, **3**, 1745–1752.
169 A. R. Liu, C. Li, H. Bai and G. Q. Shi, *J. Phys. Chem. C*, 2010, **114**, 22783–22789.
170 K. H. Chang, C. C. Hu and C. Y. Chou, *Chem. Mater.*, 2007, **19**, 2112–2119.
171 X. Qin, S. Durbach and G. T. Wu, *Carbon*, 2004, **42**, 451–453.
172 Z. S. Wu, D. W. Wang, W. Ren, J. Zhao, G. Zhou, F. Li and H. M. Cheng, *Adv. Funct. Mater.*, 2010, **20**, 3595–3602.
173 J. B. Fei, Y. Cui, X. H. Yan, W. Qi, Y. Yang, K. W. Wang, Q. He and J. B. Li, *Adv. Mater.*, 2008, **20**, 452–456.
174 F. Jiao and P. G. Bruce, *Adv. Mater.*, 2007, **19**, 657–660.
175 X. Lu, T. Zhai, X. Zhang, Y. Shen, L. Yuan, B. Hu, L. Gong, J. Chen, Y. Gao, J. Zhou, Y. Tong and Z. L. Wang, *Adv. Mater.*, 2012, **24**, 938–944.
176 Z. J. Fan, J. Yan, T. Wei, L. J. Zhi, G. Q. Ning, T. Y. Li and F. Wei, *Adv. Funct. Mater.*, 2011, **21**, 2366–2375.
177 J. Yan, Z. J. Fan, T. Wei, W. Z. Qian, M. L. Zhang and F. Wei, *Carbon*, 2010, **48**, 3825–3833.
178 S. Chen, J. W. Zhu, X. D. Wu, Q. F. Han and X. Wang, *ACS Nano*, 2010, **4**, 2822–2830.
179 Z. S. Wu, W. C. Ren, D. W. Wang, F. Li, B. L. Liu and H. M. Cheng, *ACS Nano*, 2010, **4**, 5835–5842.
180 X. H. Xia, J. P. Tu, Y. J. Mai, R. Chen, X. L. Wang, C. D. Gu and X. B. Zhao, *Chem.–Eur. J.*, 2011, **17**, 10898–10905.
181 M. S. Wu, Y. P. Lin, C. H. Lin and J. T. Lee, *J. Mater. Chem.*, 2012, **22**, 2442–2448.
182 B. Zhao, J. S. Song, P. Liu, W. W. Xu, T. Fang, Z. Jiao, H. J. Zhang and Y. Jiang, *J. Mater. Chem.*, 2011, **21**, 18792–18798.
183 C. Yuan, L. Yang, L. Hou, J. Li, Y. Sun, X. Zhang, L. Shen, X. Lu, S. Xiong and X. W. Lou, *Adv. Funct. Mater.*, 2012, **22**, 2560–2566.

184 X.-C. Dong, H. Xu, X.-W. Wang, Y.-X. Huang, M. B. Chan-Park, H. Zhang, L.-H. Wang, W. Huang and P. Chen, *ACS Nano*, 2012, **6**, 3206–3213.
185 J. A. Jiang, J. P. Liu, R. M. Ding, J. H. Zhu, Y. Y. Li, A. Z. Hu, X. Li and X. T. Huang, *ACS Appl. Mater. Interfaces*, 2011, **3**, 99–103.
186 J. Yan, Z. Fan, W. Sun, G. Ning, T. Wei, Q. Zhang, R. Zhang, L. Zhi and F. Wei, *Adv. Funct. Mater.*, 2012, **22**, 2632–2641.
187 H. L. Wang, J. T. Robinson, G. Diankov and H. J. Dai, *J. Am. Chem. Soc.*, 2010, **132**, 3270–3271.
188 H. L. Wang, H. S. Casalongue, Y. Y. Liang and H. J. Dai, *J. Am. Chem. Soc.*, 2010, **132**, 7472–7477.
189 X. Chen, X. J. Huang, L. T. Kong, Z. Guo, X. C. Fu, M. Q. Li and J. H. Liu, *J. Mater. Chem.*, 2010, **20**, 352–359.
190 C. J. Shih, A. Vijayaraghavan, R. Krishnan, R. Sharma, J. H. Han, M. H. Ham, Z. Jin, S. C. Lin, G. L. C. Paulus, N. F. Reuel, Q. H. Wang, D. Blankschtein and M. S. Strano, *Nat. Nanotechnol.*, 2011, **6**, 439–445.
191 S. Chen, J. W. Zhu and X. Wang, *J. Phys. Chem. C*, 2010, **114**, 11829–11834.
192 M. Li, J. E. Zhu, L. Zhang, X. Chen, H. Zhang, F. Zhang, S. Xu and D. G. Evans, *Nanoscale*, 2011, **3**, 4240–4246.
193 L. B. Hu, M. Pasta, F. La Mantia, L. F. Cui, S. Jeong, H. D. Deshazer, J. W. Choi, S. M. Han and Y. Cui, *Nano Lett.*, 2010, **10**, 708–714.
194 C. Z. Meng, C. H. Liu, L. Z. Chen, C. H. Hu and S. S. Fan, *Nano Lett.*, 2010, **10**, 4025–4031.
195 L. B. Hu and Y. Cui, *Energy Environ. Sci.*, 2012, **5**, 6423–6435.
196 G. Eda, G. Fanchini and M. Chhowalla, *Nat. Nanotechnol.*, 2008, **3**, 270–274.
197 Y. X. Xu, H. Bai, G. W. Lu, C. Li and G. Q. Shi, *J. Am. Chem. Soc.*, 2008, **130**, 5856–5857.
198 A. P. Yu, I. Roes, A. Davies and Z. W. Chen, *Appl. Phys. Lett.*, 2010, **96**, 253105.
199 Z. Weng, Y. Su, D. W. Wang, F. Li, J. H. Du and H. M. Cheng, *Adv. Energy Mater.*, 2011, **1**, 917–922.
200 Z. P. Li, Y. J. Mi, X. H. Liu, S. Liu, S. R. Yang and J. Q. Wang, *J. Mater. Chem.*, 2011, **21**, 14706–14711.
201 X. Y. Dong, L. Wang, D. Wang, C. Li and J. Jin, *Langmuir*, 2012, **28**, 293–298.
202 G. Yu, L. Hu, M. Vosgueritchian, H. Wang, X. Xie, J. R. McDonough, X. Cui, Y. Cui and Z. Bao, *Nano Lett.*, 2011, **11**, 2905–2911.
203 B. Scrosati and J. Garche, *J. Power Sources*, 2010, **195**, 2419–2430.
204 B. K. Guo, H. Xu, X. Y. Wang and L. X. Xiao, *Lithium ion batteries*, Central south university press, Changsha, 2002, pp. 7–11.
205 C. Liu, F. Li, L. P. Ma and H. M. Cheng, *Adv. Mater.*, 2010, **22**, E28–E62.
206 J. R. Dahn, T. Zheng, Y. H. Liu and J. S. Xue, *Science*, 1995, **270**, 590–593.
207 K. Sato, M. Noguchi, A. Demachi, N. Oki and M. Endo, *Science*, 1994, **264**, 556–558.
208 E. Pollak, B. Geng, K. J. Jeon, I. T. Lucas, T. J. Richardson, F. Wang and R. Kostecki, *Nano Lett.*, 2010, **10**, 3386–3388.
209 C. Uthaisar and V. Barone, *Nano Lett.*, 2010, **10**, 2838–2842.
210 P. Guo, H. Song and X. Chen, *Electrochem. Commun.*, 2009, **11**, 1320–1324.
211 P. Lian, X. Zhu, S. Liang, Z. Li, W. Yang and H. Wang, *Electrochim. Acta*, 2010, **55**, 3909–3914.
212 G. X. Wang, X. P. Shen, J. Yao and J. Park, *Carbon*, 2009, **47**, 2049–2053.
213 E. J. Yoo, J. Kim, E. Hosono, H. Zhou, T. Kudo and I. Honma, *Nano Lett.*, 2008, **8**, 2277–2282.
214 X. Zhao, C. M. Hayner, M. C. Kung and H. H. Kung, *ACS Nano*, 2011, **5**, 8739–8749.
215 T. Bhardwaj, A. Antic, B. Pavan, V. Barone and B. D. Fahlman, *J. Am. Chem. Soc.*, 2010, **132**, 12556–12558.
216 C. K. Chan, H. L. Peng, G. Liu, K. McIlwrath, X. F. Zhang, R. A. Huggins and Y. Cui, *Nat. Nanotechnol.*, 2008, **3**, 31–35.
217 H. C. Tao, L. Z. Fan, Y. Mei and X. Qu, *Electrochem. Commun.*, 2011, **13**, 1332–1335.
218 S. L. Chou, J. Z. Wang, M. Choucair, H. K. Liu, J. A. Stride and S. X. Dou, *Electrochem. Commun.*, 2010, **12**, 303–306.
219 J. K. Lee, K. B. Smith, C. M. Hayner and H. H. Kung, *Chem. Commun.*, 2010, **46**, 2025–2027.
220 H. F. Xiang, K. Zhang, G. Ji, J. Y. Lee, C. J. Zou, X. D. Chen and J. S. Wu, *Carbon*, 2011, **49**, 1787–1796.
221 X. S. Zhou, Y. X. Yin, L. J. Wan and Y. G. Guo, *Chem. Commun.*, 2012, **48**, 2198–2200.
222 S. N. Yang, G. R. Li, Q. Zhu and Q. M. Pan, *J. Mater. Chem.*, 2012, **22**, 3420–3425.
223 X. L. Wang and W. Q. Han, *ACS Appl. Mater. Interfaces*, 2010, **2**, 3709–3713.
224 K. Evanoff, A. Magasinski, J. B. Yang and G. Yushin, *Adv. Energy Mater.*, 2011, **1**, 495–498.
225 X. Zhao, C. M. Hayner, M. C. Kung and H. H. Kung, *Adv. Energy Mater.*, 2011, **1**, 1079–1084.
226 G. Wang, B. Wang, X. Wang, J. Park, S. Dou, H. Ahn and K. Kim, *J. Mater. Chem.*, 2009, **19**, 8378–8384.
227 C. Wang, Y. Zhou, M. Y. Ge, X. B. Xu, Z. L. Zhang and J. Z. Jiang, *J. Am. Chem. Soc.*, 2010, **132**, 46–47.
228 Z. Du, X. Yin, M. Zhang, Q. Hao, Y. Wang and T. Wang, *Mater. Lett.*, 2010, **64**, 2076–2079.
229 M. Winter and J. O. Besenhard, *Electrochim. Acta*, 1999, **45**, 31–50.
230 L. Ji, Z. Tan, T. Kuykendall, E. J. An, Y. Fu, V. Battaglia and Y. Zhang, *Energy Environ. Sci.*, 2011, **4**, 3611–3616.
231 Z. H. Wen, S. M. Cui, H. J. Kim, S. Mao, K. H. Yu, G. H. Lu, H. H. Pu, O. Mao and J. H. Chen, *J. Mater. Chem.*, 2012, **22**, 3300–3306.
232 J. Yao, X. Shen, B. Wang, H. Liu and G. Wang, *Electrochem. Commun.*, 2009, **11**, 1849–1852.
233 S. M. Paek, E. J. Yoo and I. Honma, *Nano Lett.*, 2008, **9**, 72–75.
234 L. S. Zhang, L. Y. Jiang, H. J. Yan, W. D. Wang, W. Wang, W. G. Song, Y. G. Guo and L. J. Wan, *J. Mater. Chem.*, 2010, **20**, 5462–5467.
235 C. H. Xu, J. Sun and L. Gao, *J. Mater. Chem.*, 2012, **22**, 975–979.
236 C. H. Xu, J. Sun and L. Gao, *Nanoscale*, 2012, **4**, 5425–5430.

237 Z. S. Wu, W. C. Ren, L. Wen, L. B. Gao, J. P. Zhao, Z. P. Chen, G. M. Zhou, F. Li and H. M. Cheng, *ACS Nano*, 2010, **4**, 3187–3194.
238 D. H. Wang, D. W. Choi, J. Li, Z. G. Yang, Z. M. Nie, R. Kou, D. H. Hu, C. M. Wang, L. V. Saraf, J. G. Zhang, I. A. Aksay and J. Liu, *ACS Nano*, 2009, **3**, 907–914.
239 G. Zhou, D.-W. Wang, L.-C. Yin, N. Li, F. Li and H.-M. Cheng, *ACS Nano*, 2012, **6**, 3214–3223.
240 G. M. Zhou, D. W. Wang, F. Li, L. L. Zhang, N. Li, Z. S. Wu, L. Wen, G. Q. Lu and H. M. Cheng, *Chem. Mater.*, 2010, **22**, 5306–5313.
241 J. Z. Wang, C. Zhong, D. Wexler, N. H. Idris, Z. X. Wang, L. Q. Chen and H. K. Liu, *Chem.–Eur. J.*, 2011, **17**, 661–667.
242 Z. Y. Wang, L. Zhou and X. W. Lou, *Adv. Mater.*, 2012, **24**, 1903–1911.
243 H. Kim, D. H. Seo, S. W. Kim, J. Kim and K. Kang, *Carbon*, 2011, **49**, 326–332.
244 L. Q. Tao, J. T. Zai, K. X. Wang, H. J. Zhang, M. Xu, J. Shen, Y. Z. Su and X. F. Qian, *J. Power Sources*, 2012, **202**, 230–235.
245 B. Li, H. Cao, J. Shao, G. Li, M. Qu and G. Yin, *Inorg. Chem.*, 2011, **50**, 1628–1632.
246 S. Q. Chen and Y. Wang, *J. Mater. Chem.*, 2010, **20**, 9735–9739.
247 Y. C. Qiu, K. Y. Yan, S. H. Yang, L. M. Jin, H. Deng and W. S. Li, *ACS Nano*, 2010, **4**, 6515–6526.
248 S. J. Ding, J. S. Chen, D. Y. Luan, F. Y. C. Boey, S. Madhavi and X. W. Lou, *Chem. Commun.*, 2011, **47**, 5780–5782.
249 J. Zhong, X. L. Wang, X. H. Xia, C. D. Gu, J. Y. Xiang, J. Zhang and J. P. Tu, *J. Alloys Compd.*, 2011, **509**, 3889–3893.
250 C. H. Xu, J. Sun and L. A. Gao, *J. Power Sources*, 2011, **196**, 5138–5142.
251 Y. J. Mai, S. J. Shi, D. Zhang, Y. Lu, C. D. Gu and J. P. Tu, *J. Power Sources*, 2012, **204**, 155–161.
252 X. J. Zhu, J. Hu, H. L. Dai, L. Ding and L. Jiang, *Electrochim. Acta*, 2012, **64**, 23–28.
253 L. Q. Tao, J. T. Zai, K. X. Wang, Y. H. Wan, H. J. Zhang, C. Yu, Y. L. Xiao and X. F. Qian, *RSC Adv.*, 2012, **2**, 3410–3415.
254 P. Lian, X. Zhu, H. Xiang, Z. Li, W. Yang and H. Wang, *Electrochim. Acta*, 2010, **56**, 834–840.
255 M. Zhang, D. Lei, X. Yin, L. Chen, Q. Li, Y. Wang and T. Wang, *J. Mater. Chem.*, 2010, **20**, 5538–5543.
256 D. Chen, G. Ji, Y. Ma, J. Y. Lee and J. Lu, *ACS Appl. Mater. Interfaces*, 2011, **3**, 3078–3083.
257 B. Li, H. Cao, J. Shao and M. Qu, *Chem. Commun.*, 2011, **47**, 10374–10376.
258 J. Zhou, H. Song, L. Ma and X. Chen, *RSC Adv.*, 2011, **1**, 782–791.
259 J. T. Zai, C. Yu, Q. Zou, L. Q. Tao, K. X. Wang, Q. Y. Han, B. Li, Y. L. Xiao, X. F. Qian and R. R. Qi, *RSC Adv.*, 2012, **2**, 4397–4403.
260 L. M. Dai, D. W. Chang, J. B. Baek and W. Lu, *Small*, 2012, **8**, 1130–1166.
261 K. Evanoff, J. Khan, A. A. Balandin, A. Magasinski, W. J. Ready, T. F. Fuller and G. Yushin, *Adv. Mater.*, 2012, **24**, 533–537.
262 C. H. Xu, J. Sun and L. Gao, *J. Phys. Chem. C*, 2009, **113**, 20509–20513.
263 Y. Wang and G. Z. Cao, *Adv. Mater.*, 2008, **20**, 2251–2269.
264 K. Park, J. Son, H. Chung, S. Kim, C. Lee and H. Kim, *Electrochem. Commun.*, 2003, **5**, 839–842.
265 Y. F. Tang, F. Q. Huang, H. Bi, Z. Q. Liu and D. Y. Wan, *J. Power Sources*, 2012, **203**, 130–134.
266 Y. Ding, Y. Jiang, F. Xu, J. Yin, H. Ren, Q. Zhuo, Z. Long and P. Zhang, *Electrochem. Commun.*, 2010, **12**, 10–13.
267 Y. Wang, Z. S. Feng, J. J. Chen and C. Zhang, *Mater. Lett.*, 2012, **71**, 54–56.
268 C. Su, X. D. Bu, L. H. Xu, J. L. Liu and C. Zhang, *Electrochim. Acta*, 2012, **64**, 190–195.
269 H. J. Liu and Y. Y. Xia, *Progress in Chemistry*, 2011, **23**, 595–604.
270 G. G. Amatucci, F. Badway, A. Du Pasquier and T. Zheng, *J. Electrochem. Soc.*, 2001, **148**, A930–A939.
271 Q. T. Qu, P. Zhang, B. Wang, Y. H. Chen, S. Tian, Y. P. Wu and R. Holze, *J. Phys. Chem. C*, 2009, **113**, 14020–14027.
272 Q. T. Qu, L. J. Fu, X. Y. Zhan, D. Samuelis, J. Maier, L. Li, S. Tian, Z. H. Li and Y. P. Wu, *Energy Environ. Sci.*, 2011, **4**, 3985–3990.
273 L. Wang, D. Wang, X. Y. Dong, Z. J. Zhang, X. F. Pei, X. J. Chen, B. A. Chen and J. A. Jin, *Chem. Commun.*, 2011, **47**, 3556–3558.
274 Z. Gao, J. Wang, Z. S. Li, W. L. Yang, B. Wang, M. J. Hou, Y. He, Q. Liu, T. Mann, P. P. Yang, M. L. Zhang and L. H. Liu, *Chem. Mater.*, 2011, **23**, 3509–3516.
275 J. Zhang, J. Jiang, H. Li and X. S. Zhao, *Energy Environ. Sci.*, 2011, **4**, 4009–4015.
276 L. Y. Yuan, X. H. Lu, X. Xiao, T. Zhai, J. J. Dai, F. C. Zhang, B. Hu, X. Wang, L. Gong, J. Chen, C. G. Hu, Y. X. Tong, J. Zhou and Z. L. Wang, *ACS Nano*, 2012, **6**, 656–661.
277 C. X. Guo, M. Wang, T. Chen, X. W. Lou and C. M. Li, *Adv. Energy Mater.*, 2011, **1**, 736–741.
278 S. Y. Han, I. Y. Kim, K. Y. Jo and S. J. Hwang, *J. Phys. Chem. C*, 2012, **116**, 7269–7279.
279 H. Liu and W. Yang, *Energy Environ. Sci.*, 2011, **4**, 4000–4008.
280 J. Zhang, J. Jiang, H. Li and X. S. Zhao, *Energy Environ. Sci.*, 2011, **4**, 4009–4015.
281 L. Mao, K. Zhang, H. S. O. Chan and J. S. Wu, *J. Mater. Chem.*, 2012, **22**, 1845–1851.
282 L. Shen, C. Yuan, H. Luo, X. Zhang, S. Yang and X. Lu, *Nanoscale*, 2011, **3**, 572–574.
283 M. D. Stoller, S. Murali, N. Quarles, Y. W. Zhu, J. R. Potts, X. J. Zhu, H. W. Ha and R. S. Ruoff, *Phys. Chem. Chem. Phys.*, 2012, **14**, 3388–3391.
284 W. H. Shin, H. M. Jeong, B. G. Kim, J. K. Kang and J. W. Choi, *Nano Lett.*, 2012, **12**, 2283–2288.
285 M. S. Park, Y. G. Lim, J. H. Kim, Y. J. Kim, J. Cho and J. S. Kim, *Adv. Energy Mater.*, 2011, **1**, 1002–1006.
286 D. W. Liu, B. B. Garcia, Q. F. Zhang, Q. Guo, Y. H. Zhang, S. Sepehri and G. Z. Cao, *Adv. Funct. Mater.*, 2009, **19**, 1015–1023.
287 B. Dunn, H. Kamath and J. M. Tarascon, *Science*, 2011, **334**, 928–935.

288 X. L. Ji, K. T. Lee and L. F. Nazar, *Nat. Mater.*, 2009, **8**, 500–506.
289 A. Kraytsberg and Y. Ein-Eli, *J. Power Sources*, 2011, **196**, 886–893.
290 E. Yoo and H. S. Zhou, *ACS Nano*, 2011, **5**, 3020–3026.
291 J. Xiao, D. Mei, X. Li, W. Xu, D. Wang, G. L. Graff, W. D. Bennett, Z. Nie, L. V. Saraf, I. A. Aksay, J. Liu and J.-G. Zhang, *Nano Lett.*, 2011, **11**, 5071–5078.
292 E. Yoo, J. Nakamura and H. Zhou, *Energy Environ. Sci.*, 2012, **5**, 3020–3026.
293 B. Wang, Y. F. Ma, Y. P. Wu, N. Li, Y. Huang and Y. S. Chen, *Carbon*, 2009, **47**, 2112–2115.
294 X. L. Wei, M. S. Wang, Y. Bando and D. Golberg, *J. Am. Chem. Soc.*, 2010, **132**, 13592–13593.
295 I. Gierz, C. Riedl, U. Starke, C. R. Ast and K. Kern, *Nano Lett.*, 2008, **8**, 4603–4607.
296 T. O. Wehling, K. S. Novoselov, S. V. Morozov, E. E. Vdovin, M. I. Katsnelson, A. K. Geim and A. I. Lichtenstein, *Nano Lett.*, 2008, **8**, 173–177.
297 Z. Yang, Z. Yao, G. F. Li, G. Y. Fang, H. G. Nie, Z. Liu, X. M. Zhou, X. Chen and S. M. Huang, *ACS Nano*, 2012, **6**, 205–211.
298 J. Y. Dai, J. M. Yuan and P. Giannozzi, *Appl. Phys. Lett.*, 2009, **95**, 232105.
299 P. A. Denis, *Chem. Phys. Lett.*, 2010, **492**, 251–257.
300 P. A. Denis, R. Faccio and A. W. Mombru, *ChemPhysChem*, 2009, **10**, 715–722.
301 Y. C. Lu, H. A. Gasteiger, M. C. Parent, V. Chiloyan and Y. Shao-Horn, *Electrochem. Solid-State Lett.*, 2010, **13**, A69–A72.
302 R. Padbury and X. W. Zhang, *J. Power Sources*, 2011, **196**, 4436–4444.
303 Y. C. Lu, Z. C. Xu, H. A. Gasteiger, S. Chen, K. Hamad-Schifferli and Y. Shao-Horn, *J. Am. Chem. Soc.*, 2010, **132**, 12170–12171.
304 Y. Liang, Y. Li, H. Wang, J. Zhou, J. Wang, T. Regier and H. Dai, *Nat. Mater.*, 2011, **10**, 780–786.
305 A. Debart, A. J. Paterson, J. Bao and P. G. Bruce, *Angew. Chem., Int. Ed.*, 2008, **47**, 4521–4524.
306 G. Girishkumar, B. McCloskey, A. C. Luntz, S. Swanson and W. Wilcke, *J. Phys. Chem. Lett.*, 2010, **1**, 2193–2203.
307 D. Zhang, R. S. Li, T. Huang and A. S. Yu, *J. Power Sources*, 2010, **195**, 1202–1206.
308 J. Suntivich, H. A. Gasteiger, N. Yabuuchi, H. Nakanishi, J. B. Goodenough and Y. Shao-Horn, *Nat. Chem.*, 2011, **3**, 546–550.
309 G. J. la O, S. J. Ahn, E. Crumlin, Y. Orikasa, M. D. Biegalski, H. M. Christen and Y. Shao-Horn, *Angew. Chem., Int. Ed.*, 2010, **49**, 5344–5347.
310 E. Mutoro, E. J. Crumlin, M. D. Biegalski, H. M. Christen and Y. Shao-Horn, *Energy Environ. Sci.*, 2011, **4**, 3689–3696.
311 P. G. Bruce, S. A. Freunberger, L. J. Hardwick and J.-M. Tarascon, *Nat. Mater.*, 2012, **11**, 19–29.
312 J. Njoroge, *MRS Bull.*, 2011, **36**, 669.
313 J. Schuster, G. He, B. Mandlmeier, T. Yim, K. T. Lee, T. Bein and L. F. Nazar, *Angew. Chem., Int. Ed.*, 2012, **51**, 3591–3595.
314 L. Xiao, Y. Cao, J. Xiao, B. Schwenzer, M. H. Engelhard, L. V. Saraf, Z. Nie, G. J. Exarhos and J. Liu, *Adv. Mater.*, 2012, **24**, 1176–1181.
315 C. D. Liang, N. J. Dudney and J. Y. Howe, *Chem. Mater.*, 2009, **21**, 4724–4730.
316 J. Z. Wang, L. Lu, M. Choucair, J. A. Stride, X. Xu and H. K. Liu, *J. Power Sources*, 2011, **196**, 7030–7034.
317 H. L. Wang, Y. Yang, Y. Y. Liang, J. T. Robinson, Y. G. Li, A. Jackson, Y. Cui and H. J. Dai, *Nano Lett.*, 2011, **11**, 2644–2647.
318 S. Evers and L. F. Nazar, *Chem. Commun.*, 2012, **48**, 1233–1235.
319 L. Yin, J. Wang, F. Lin, J. Yang and Y. Nuli, *Energy Environ. Sci.*, 2012, **5**, 6966–6972.
320 X. L. Ji, S. Evers, R. Black and L. F. Nazar, *Nat. Commun.*, 2011, **2**, 325.
321 L. Ji, M. Rao, H. Zheng, L. Zhang, Y. Li, W. Duan, J. Guo, E. J. Cairns and Y. Zhang, *J. Am. Chem. Soc.*, 2011, **133**, 18522–18525.